Global Change Biology WILEY

Greenhouse gas production and lipid biomarker distribution in Yedoma and Alas thermokarst lake sediments in Eastern Siberia

Loeka L. Jongejans[1,2] | Susanne Liebner[3,4] | Christian Knoblauch[5,6] | Kai Mangelsdorf[7] | Mathias Ulrich[8] | Guido Grosse[1,2] | George Tanski[1,9] | Alexander N. Fedorov[10,11] | Pavel Ya. Konstantinov[10] | Torben Windirsch[1,2] | Julia Wiedmann[1,12] | Jens Strauss[1]

[1]Alfred Wegener Institute Helmholtz Center for Polar and Marine Research, Permafrost Research Section, Potsdam, Germany

[2]Institute of Geosciences, University of Potsdam, Potsdam, Germany

[3]Section Geomicrobiology, GFZ German Research Center for Geosciences, Potsdam, Germany

[4]Institute of Biochemistry and Biology, University of Potsdam, Potsdam, Germany

[5]Institute of Soil Science, Universität Hamburg, Hamburg, Germany

[6]Center for Earth System Research and Sustainability, Hamburg, Germany

[7]Section Organic Geochemistry, GFZ German Research Center for Geosciences, Potsdam, Germany

[8]Institute for Geography, University of Leipzig, Leipzig, Germany

[9]Department of Earth Science, Vrije Universiteit Amsterdam, Amsterdam, Netherlands

[10]Melnikov Permafrost Institute, Laboratory of General Geocryology, Siberian Branch Russian Academy of Sciences, Yakutsk, Russia

[11]BEST International Centre, North-Eastern Federal University, Yakutsk, Russia

[12]Baugrund-Ingenieurbüro GmbH Maul und Partner, Potsdam, Germany

Correspondence
Loeka L. Jongejans, Alfred Wegener Institute Helmholtz Center for Polar and Marine Research, Permafrost Research Section, 14473 Potsdam, Germany.
Email: loeka.jongejans@awi.de

Abstract

Permafrost thaw leads to thermokarst lake formation and talik growth tens of meters deep, enabling microbial decomposition of formerly frozen organic matter (OM). We analyzed two 17-m-long thermokarst lake sediment cores taken in Central Yakutia, Russia. One core was from an Alas lake in a Holocene thermokarst basin that underwent multiple lake generations, and the second core from a young Yedoma upland lake (formed ~70 years ago) whose sediments have thawed for the first time since deposition. This comparison provides a glance into OM fate in thawing Yedoma deposits. We analyzed total organic carbon (TOC) and dissolved organic carbon (DOC) content, n-alkane concentrations, and bacterial and archaeal membrane markers. Furthermore, we conducted 1-year-long incubations (4°C, dark) and measured anaerobic carbon dioxide (CO_2) and methane (CH_4) production. The sediments from both cores contained little TOC (0.7 ± 0.4 wt%), but DOC values were relatively high, with the highest values in the frozen Yedoma lake sediments (1620 mg L^{-1}). Cumulative greenhouse gas (GHG) production after 1 year was highest in the Yedoma lake sediments

($226 \pm 212\ \mu g\ CO_2$-C g^{-1} dw, $28 \pm 36\ \mu g\ CH_4$-C g^{-1} dw) and 3 and 1.5 times lower in the Alas lake sediments, respectively ($75 \pm 76\ \mu g\ CO_2$-C g^{-1} dw, $19 \pm 29\ \mu g\ CH_4$-C g^{-1} dw). The highest CO_2 production in the frozen Yedoma lake sediments likely results from decomposition of readily bioavailable OM, while highest CH_4 production in the non-frozen top sediments of this core suggests that methanogenic communities established upon thaw. The lower GHG production in the non-frozen Alas lake sediments resulted from advanced OM decomposition during Holocene talik development. Furthermore, we found that drivers of CO_2 and CH_4 production differ following thaw. Our results suggest that GHG production from TOC-poor mineral deposits, which are widespread throughout the Arctic, can be substantial. Therefore, our novel data are relevant for vast ice-rich permafrost deposits vulnerable to thermokarst formation.

KEYWORDS
anaerobic, greenhouse gases, incubation experiments, lipid biomarkers, organic matter degradation, permafrost thaw, talik, Yakutia

1 | INTRODUCTION

Rapid warming of the Arctic results in permafrost warming (Biskaborn et al., 2019) and thaw, enabling microbial decomposition of previously frozen organic matter (OM; Schuur et al., 2008; Walter Anthony et al., 2016). Soil organic carbon (OC) that has been stored for millennia could be released to the atmosphere as greenhouse gases (GHGs). OC release from permafrost regions will continue gradually with ongoing warming, thereby accelerating warming (Schuur et al., 2015). Factors controlling GHG release from thawing permafrost are complex and therefore not fully considered by most climate models (Turetsky et al., 2020).

Thermokarst lake and talik formation is the most common expression of deep permafrost degradation (>10 m depth; Grosse et al., 2013). Ground subsidence following thawing of ice-rich ground beneath the lake leads to lake formation. A positive downward heat flux from the water further enhances thaw and leads to the formation of a talik. After lake drainage or desiccation, a subaerial thermokarst lake basin remains, which is called an alas (Soloviev, 1973). Consequently, the talik can refreeze and OC becomes freeze-locked again. Thermokarst and talik formation, especially in ice-rich Late Pleistocene Yedoma deposits, result in deep thaw and subsequent ground subsidence. Aside from being ice-rich and susceptible to ground subsidence, deep Yedoma deposits (>25 m depth) are an important pool of permafrost OM (Schirrmeister et al., 2013; Strauss et al., 2017). In contrast, gradual top-down thawing, such as active layer deepening, affects only centimeters per decade (Grosse et al., 2011; Turetsky et al., 2020). Turetsky et al. (2020) estimated that abrupt thaw processes, such as thermokarst lake development, could lead to an additional net OC release from permafrost regions of 80 ± 19 Pg by 2300 under RCP 8.5. Thermokarst development in Yedoma regions, therefore, contributes globally relevant GHG emissions to the active carbon cycle (Turetsky et al., 2020).

The amount of OM that can be mobilized upon thaw is highly dependent on the state of OM degradation. Several studies have analyzed permafrost OM on a molecular level using lipid biomarkers

to assess OM degradability (Jongejans et al., 2018; Sánchez-García et al., 2014; Stapel et al., 2018; Strauss et al., 2015). The ratio of odd to even chained n-alkanes, the carbon preference index (CPI), has been used as an indicator for OM degradability where high values suggest better preserved OM (Marzi et al., 1993). Other proxies can give insights into the source of OM, such as the average chain length (ACL; Killops & Killops, 2013; Poynter & Eglinton, 1990). Branched glycerol dialkyl glycerol tetraethers (GDGTs), as well as archaeol and isoprenoid GDGTs (isoGDGT-0), are markers for past bacterial and archaeal biomass, respectively (Stapel et al., 2016; Weijers et al., 2006). In their study of Siberian Yedoma deposits, Stapel et al. (2018) found that increased concentrations of archaeal biomarkers correlated to increased OM contents, suggesting microbial activity and methane (CH_4) production during deposition.

Only a limited number of biogeochemical studies has been carried out so far on talik sediments underneath thermokarst lakes (Heslop et al., 2015, 2019; Jongejans et al., 2020; Romankevich et al., 2017; Ulyantsev et al., 2017). The study of talik sediments is however highly relevant for climate studies as it allows important insights into the pathways of previously frozen OM upon rapid thaw and thus the potential for GHG production below thermokarst lakes. While many studies suggested a higher biolability of old Yedoma OM upon thaw compared to Holocene thermokarst deposits (Dutta et al., 2006; Jongejans et al., 2018; Lee et al., 2012; Neubauer, 2016; Schuur et al., 2009; Strauss et al., 2015, 2017; Zimov et al., 2006), a few studies showed opposite findings (Kuhry et al., 2020; Schädel et al., 2014). Furthermore, climatic conditions during permafrost formation were shown to play a crucial role for OM decomposition after thaw (Knoblauch et al., 2013; Walz et al., 2018). In addition, studies of biolability of dissolved OC (DOC) showed that old OC was more biolabile compared to modern OC (Mann et al., 2015; Vonk et al., 2013).

Schädel et al. (2014, 2016) and Treat et al. (2015) compiled an overview of incubation studies of permafrost regions. Many of these incubation experiments included subsurface sediments (<1 m depth; e.g., Čapek et al., 2015; Diáková et al., 2016; Elberling et al., 2013;

Estop-Aragonés & Blodau, 2012; Waldrop et al., 2010) and only few studies have incubated permafrost sediments from >10 m deep (Dutta et al., 2006; Knoblauch et al., 2013; Lee et al., 2012). Even though several studies showed that aerobic decomposition released more OC than anaerobic decomposition over short time scales (months–years; Knoblauch et al., 2013; Lee et al., 2012; Schädel et al., 2016), CH_4 emissions from permafrost regions are projected to become more important on longer time scales (decades–centuries; Dean et al., 2018; Knoblauch et al., 2018). Furthermore, Knoblauch et al. (2018) showed that after multiple years, the production of carbon dioxide (CO_2) carbon equivalents is higher under anaerobic conditions when taking into account the much stronger global warming potential of CH_4 compared to CO_2 (28 over a 100-year timescale; Myhre et al., 2013). Moreover, increased thermokarst lake initiation, especially in the continuous permafrost zone (Nitze et al., 2017), might lead to a landscape-scale increase of anaerobic decomposition processes.

Here, we studied GHG production, long-chain *n*-alkanes, branched GDGTs, and archaeal microbial markers in talik sediments to determine the OM characteristics of Yedoma sediments thawed under subaquatic conditions underneath two different thermokarst lakes. We focused on the following research questions: (1) can we characterize the OM degradability of thawed Yedoma deposits using biomarker analyses and (2) how much GHG is produced in these deposits after thaw? For the first time, to the best of our knowledge, we present OC turnover data from Siberian Yedoma talik sediments. Furthermore, the combination of biomarker degradation proxies and incubation data from >10 m deep permafrost sediments that are thawed underneath a thermokarst lake is unique so far.
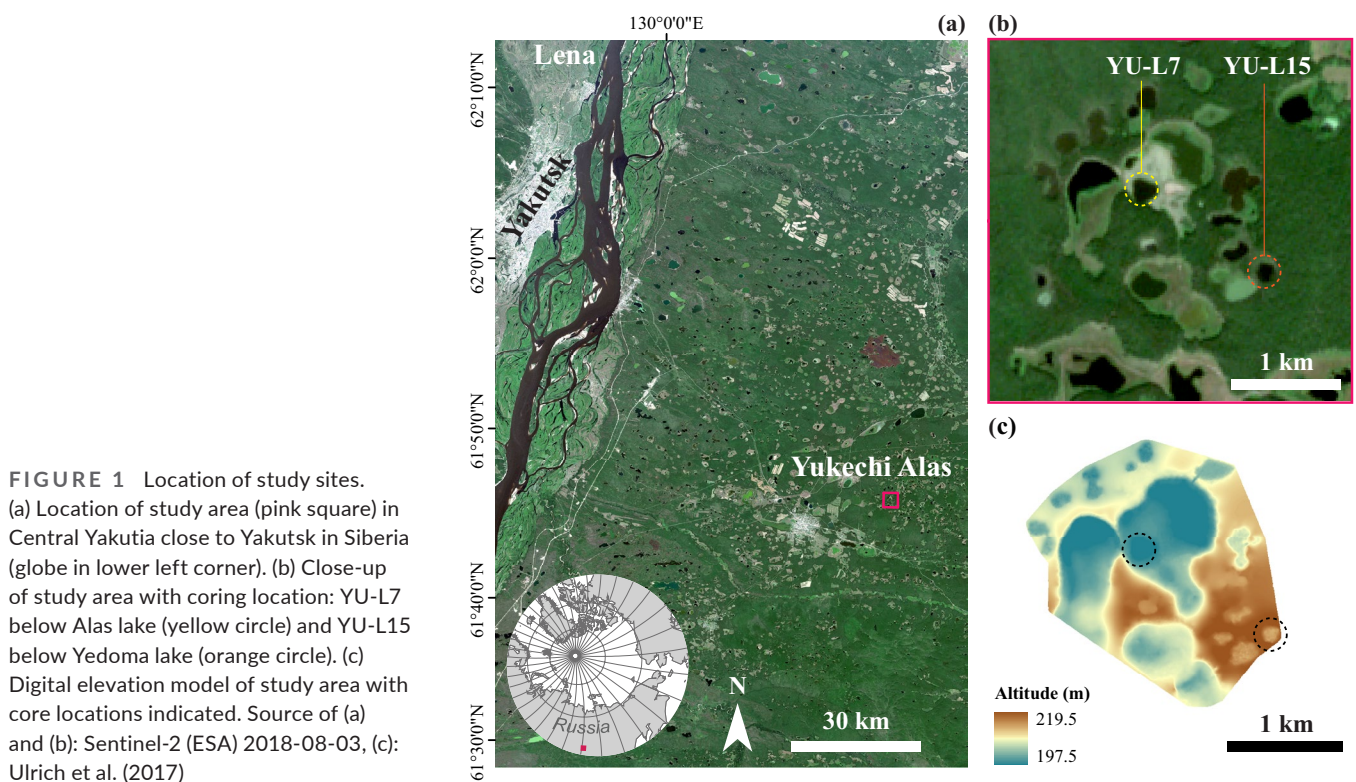
2 | MATERIALS AND METHODS

2.1 | Study area

The study site is located in Central Yakutia (Sakha Republic), East Siberia, about 80 km southeast from the city of Yakutsk (Figure 1a). The region is part of the continuous permafrost zone with permafrost reaching several hundred meters in depth. The Yukechi study site (61.76495°N, 130.46664°E) includes drained lake basins (alases) and thermokarst lakes formed in Yedoma uplands with ice-rich deposits tens of meters thick that cover about two thirds of the study area (Soloviev, 1973; Ulrich et al., 2019; Windirsch et al., 2020).

Taiga vegetation, predominantly larch trees and sparse pine and birch communities, dominate the region. Underneath the forest, the active layer reaches a thickness of ~1 m (Fedorov et al., 2014). The drained lake basins are covered by a steppe-like grass vegetation and are characterized by an active layer reaching >2 m thickness (Soloviev, 1959). The region is characterized by a strong continental climate with a mean annual air temperature of −10.7°C (mean January: −41°C, mean July: 18.5°C) and a mean annual precipitation of 246 mm (period: 1982–2012; Yakutsk Weather Station: RSM00024959; Climate-data.org, 2020).

Two different types of thermokarst lakes were selected for this study: an Alas lake and a Yedoma lake (Figure 1b). The Alas lake is located within the Yukechi Alas, which is a Holocene thermokarst basin of ~300–500 m in diameter and ~10–15 m lower compared to surrounding Yedoma uplands (Ulrich et al., 2019). The Alas lake has a diameter of ~57 m, a surface area of 1 ha and an average water depth

FIGURE 1 Location of study sites. (a) Location of study area (pink square) in Central Yakutia close to Yakutsk in Siberia (globe in lower left corner). (b) Close-up of study area with coring location: YU-L7 below Alas lake (yellow circle) and YU-L15 below Yedoma lake (orange circle). (c) Digital elevation model of study area with core locations indicated. Source of (a) and (b): Sentinel-2 (ESA) 2018-08-03, (c): Ulrich et al. (2017)

of 1.9 m (measured in summer 2014). The Yedoma thermokarst lake is a younger lake and is located on the Yedoma uplands. Its lake level lies approximately 18 m higher than the Alas lake level (Figure 1c). With a diameter of ~43 m and surface area of 0.6 ha, the Yedoma lake is smaller than the Alas lake but deeper (average water depth of 3.7 m). Using historical aerial imagery, this lake was estimated to be about 70 years old and developed in a small forest-free grassland area (Ulrich et al., 2017).

Thermokarst lake development in the Yukechi Alas has been monitored by the Melnikov Permafrost Institute in Yakutsk since 1992 (Fedorov & Konstantinov, 2003). Previous research by Ulrich et al. (2017) included remote sensing as well as field and statistical analysis of thermokarst lake change in the Yukechi Alas. In addition, Windirsch et al. (2020) assessed the local sediment genesis and its effect on permafrost carbon storage by analyzing sediment cores taken from Yedoma upland sediments in the close vicinity of the studied Yedoma lake YU-L15 (140 m SSW) and Alas deposits adjacent to Alas lake YU-L7 (110 m NNE; Figure S1).

2.2 | Field work

During the field campaign to Yukechi in March 2015, we retrieved two sediment cores from the bottom of two thermokarst lakes (Figure 1b). Drilling was carried out from the lake ice using a URB2-4T drilling rig mounted on a truck. The cores were drilled with 15.7 cm diameter for the uppermost parts and 8 cm in diameter in the lower parts. The sediment cores were removed from the core barrel using compressed air. Sediment core YU-L7 was 17.7 m long and retrieved from the Alas lake (61.76397°N, 130.46442°E). At the sampling position, the Alas lake had an ice cover of 70 cm and a water depth of 2.3 m on March 23, 2015. The sediment core consisted entirely of unfrozen sediments, which are part of the talik underneath the thermokarst lake. Sediment core YU-L15 was 17.2 m long and taken from the Yedoma upland lake (61.76086°N, 130.47466°E). This lake had a 71-cm thick ice cover and a water depth of 4.3 m at the sampling position on March 23, 2015. The sediment core consisted of unfrozen talik sediments down to a depth of 8.1 m followed by frozen sediments below. The cores were described visually in the field, packed in plastic core wrapper, and kept frozen.

In both lakes, the ice was covered by ~35 cm snow. Directly underneath the ice cover, the pH and electrical conductivity of the lake water were respectively 8.0 and 2.45 mS cm^{-1} for the Alas lake and 8.3 and 2.29 mS cm^{-1} for the Yedoma lake.

2.3 | Laboratory analyses

We cut the sediment cores into halves with a band saw and cleaned the cutting surfaces by removing the material that was superficially thawed during the saw process. Then, we subsampled the cores for

different biogeochemical laboratory analyses (Figure 2). Ten sediment samples were taken from each core (every 1–2 m according to the stratigraphy) and analyzed for total OC (TOC) content, lipid biomarkers, and anaerobic GHG production. Radiocarbon ages from both sediment cores were published separately (Jongejans et al., 2019). Sedimentological and geochemical data are being prepared for publication in an additional study.

2.3.1 | Organic carbon content

Sediment samples (*n* = 20) were analyzed for total carbon (TC) and total nitrogen (TN) content with an elemental analyzer (VarioMAX Elementar Analyser). The total inorganic carbon (TIC) content was quantified from the amount of CO_2 that was released after sample treatment with phosphoric acid. The TOC content was calculated by subtracting the TIC from the TC and is expressed in weight percentage (wt%). We calculated the TOC to TN weight ratio, which will be referred to as the C/N ratio. This ratio can be used as OM
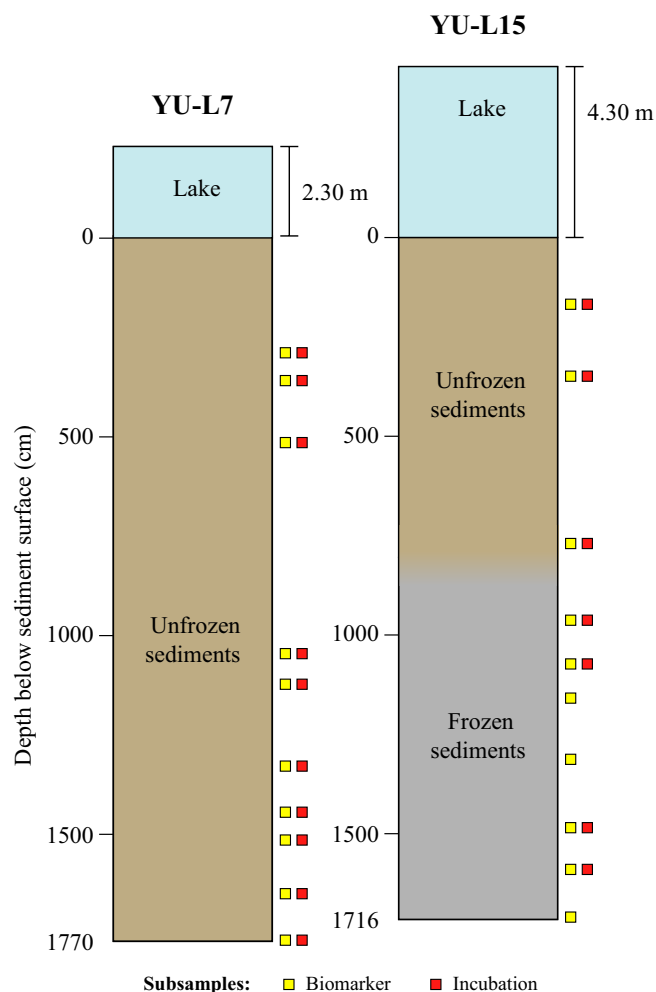

FIGURE 2 Schematic overview of sediment cores beneath Alas lake YU-L7 (left) and Yedoma lake YU-L15 (right). Subsamples were analyzed for lipid biomarkers (yellow squares) and incubation experiments (red squares)

degradation proxy where the C/N ratio decreases with decomposition (e.g., Gundelwein et al., 2007).

In addition, we extracted 3–10 ml pore water from sediment samples from both cores (n = 57) that were thawed overnight at 20°C using rhizon samplers (membrane pore size: 0.12–0.18 μm). These samples were taken from different depths than the samples for lipid biomarkers and incubations but from same stratigraphic zones. The samples were acidified with 20 μl hydrochloric acid (35%) to pH 2 and kept cool at 4°C. The dissolved OC (DOC) content was measured as non-purgeable OC fraction using a Total Organic Carbon Analyzer TOC-VCPH/CPN (Shimadzu) and is expressed in mg L^{-1}.

2.3.2 | Lipid biomarkers

Extraction and measurement
Sediment samples (n = 20) from the main stratigraphic units were analyzed for *n*-alkanes and lipid biomarkers (Figure 2). Approximately 8 g of dried, ground sediments were extracted using accelerated solvent extractions (ASE) with dichloromethane/methanol (DCM/MeOH; 99:1 v/v) using a Dionex 200 ASE Extractor. Each sample was held in a static phase (5 min heating) for 20 min (75°C, 5 MPa). Afterward, the samples were concentrated using a TurboVap500 at 42°C. We removed asphaltenes by dissolving the extracts in DCM/MeOH (99:1 v/v) and adding a 40× excess of *n*-hexane, leading to precipitation of *n*-hexane-insoluble substances. Four internal standards were added for compound quantification: 5α-androstane, ethylpyrene, 5α-androstan-17-one, and erucic acid. We separated the maltene fraction (*n*-hexane soluble compounds) by medium pressure liquid chromatography (Radke et al., 1980) into an aliphatic, aromatic and NSO (nitrogen, sulfur, and oxygen containing) fraction using *n*-hexane.

The *n*-alkanes were measured in the aliphatic fraction by gas chromatography-mass spectrometry (GC-MS) using a Trace GC Ultra coupled to a DSQ MS (Thermo Electron Corporation) with helium as carrier gas (1 ml min^{-1}). The GC was equipped with a cold injection system and a BPX5 (SGE) column (50 m × 0.22 mm × 0.25 μm). The injector temperature was programmed from 50°C to 300°C at a rate of 10°C s^{-1}. The oven was heated from its initial temperature of 50°C (1 min isothermal) to 310°C with a heating rate of 3°C min^{-1} (30 min isothermal). The MS was operated in the electron impact ionization mode at 50 eV. Full-scan mass spectra were obtained from *m/z* 50 to 600 Da with a scan rate of 2.5 scans s^{-1}. Compounds were identified and quantified using the software Xcalibur™.

The branched and isoprenoid GDGTs, as well as the dialkyl glycerol diether lipid (archaeol; Figure S2) were measured in the NSO fraction using a Shimadzu LC-10AD high-performance liquid chromatograph coupled to a Finnigan TSQ 7000 mass spectrometer via an atmospheric pressure chemical ionization interface (corona current of 5 mA [5 kV], vaporizer T of 350°C, capillary T of 200°C, nitrogen sheath gas at 60 psi, no auxiliary gas). The sample was separated at 30°C in a column oven using a Prevail Cyano column (2.1 × 150 mm, 3 μm; Alltech) equipped with a pre-column filter. Compounds were eluted isocratically with *n*-hexane (99%) and isopropanol (1%) for 5 min, followed by a linear gradient to 1.8% isopropanol in 40 min and in 1 min to 10% isopropanol. It was held for 5 min to clean the column, set back to initial conditions in 1 min, and held for 16 min for equilibration. The flow rate was set to 200 μl min^{-1}. Mass spectra were obtained by selected ion monitoring in the positive ion mode and at a scan rate of 0.33 scans s^{-1}. Compounds were identified using the software Xcalibur™ and quantified using a daily-measured external archaeol standard. Here, we present the concentration of branched GDGTs, isoGDGT-0, and archaeol.

From both sediment cores, we selected five samples for open-system pyrolysis after Horsfield et al. (1989) and Stapel et al. (2018). The bitumen-free ASE residues were pyrolyzed (temperatures: 300–600°C) and the pyrolysates, which were trapped with liquid N$_2$, were measured on a pyrolysis gas chromatograph (Agilent GC 6890A chromatograph) equipped with a flame ionization detector (Py-GC-FID). The compounds were identified and quantified relative to an *n*-butane external standard using the Agilent ChemStation software. We integrated short (C$_1$–C$_5$), intermediate (C$_6$–C$_{14}$), and longer (≥C$_{15}$) *n*-alkanes and *n*-alk-1-enes. In immature OM, these aliphatic compounds represent aliphatic side chains as well as alcohols and fatty acids formerly covalently linked via ether or ester bonds to the complex organic matrix.

Lipid biomarker indices
From the *n*-alkane concentrations, we calculated two indices. The ACL of *n*-alkanes is a measure of the chain length distribution (Poynter & Eglinton, 1990), and indicates the OM source. It was calculated according to Equation (1) where *i* is the carbon number. We focus on long-chain *n*-alkanes, which are produced by terrestrial higher plants, for example in mosses (*n*-C$_{23}$ and *n*-C$_{25}$), in leaf waxes (*n*-C$_{27}$ and *n*-C$_{29}$), and in grasses (*n*-C$_{31}$ and *n*-C$_{33}$; e.g., Ficken et al., 1998; Zech et al., 2009).

$$\text{ACL}_{23-33} = \frac{\sum i \cdot C_i}{\sum C_i}. \tag{1}$$

The CPI is an index for OM degradability. Higher values typically indicate better preserved OM and the ratio decreases with degradation (Bray & Evans, 1961; Marzi et al., 1993). The CPI was calculated according to Equation (2).

$$\text{CPI}_{23-33} = \frac{\sum \text{odd} \, C_{23-31} + \sum \text{odd} \, C_{25-33}}{2 \cdot \sum \text{even} \, C_{24-32}}. \tag{2}$$

2.3.3 | Incubations

From the 20 sediment samples, 17 samples were used in the incubation experiments to estimate GHG production from degrading OM. From each sample, we prepared three replicates for quality control. The frozen samples were thawed at 4°C overnight under an oxygen free atmosphere in a glovebox. After homogenization, approximately 10 g of sediment was weighed into 120 ml glass bottles and 10 ml

of autoclaved tap water added to each bottle with sediment. The 51 bottles were sealed with rubber stoppers and the headspace gas was exchanged with pure nitrogen to create an anaerobic atmosphere, comparable to the ambient conditions in the talik sediments below the thermokarst lakes. Samples were incubated anaerobically at 4°C for 1 year. CO_2 and CH_4 concentrations were measured biweekly in a 250-μl subsample using gas chromatography with an Agilent GC 7890A equipped with an Agilent HP-PLOT Q column. We used a thermal conductivity detector and flame ionization detector for measuring CO_2 and CH_4 concentrations, respectively, helium as a carrier gas, and an oven temperature of 100°C. From the concentrations, we calculated the average CH_4 and CO_2 production of the three replicates, which are expressed in μg CH_4-C and CO_2-C g^{-1} dry weight and g^{-1} TOC (an explanation of the calculations is provided in Supplement S1).

2.4 | Statistical analysis

We identified the stratigraphical units of the two sediment cores by constrained hierarchical clustering of all measured parameters. We carried out this statistical clustering in R v. 3.6.1 using the "chclust" function in the package "rioja" with the method "coniss" (Juggins, 2020). We calculated the correlation (Pearson) between all parameters and reported the statistically significant correlations ($p < 0.05$). Also, we compared the two sediment cores and the units using Kruskal–Wallis and Mann–Whitney Wilcoxon nonparametric tests. Using a forward-selection stepwise multiple regression, we tried to identify what parameters explained the most variance in the cumulative CH_4 and CO_2 production. We carried out the regression in R using the package "MASS" with the function "stepAIC" (Venables & Ripley, 2002) and direction "forward". This method iterates the Akaike information criteria (AIC) for the regression model when taking out one parameter at the time. The AIC statistic is a method to evaluate how well the model fits. We calculated the relative importance of the significant variables with the function "calc.relimp" from the package "relaimpo" (Groemping, 2006).

3 | RESULTS

3.1 | Organic matter characteristics

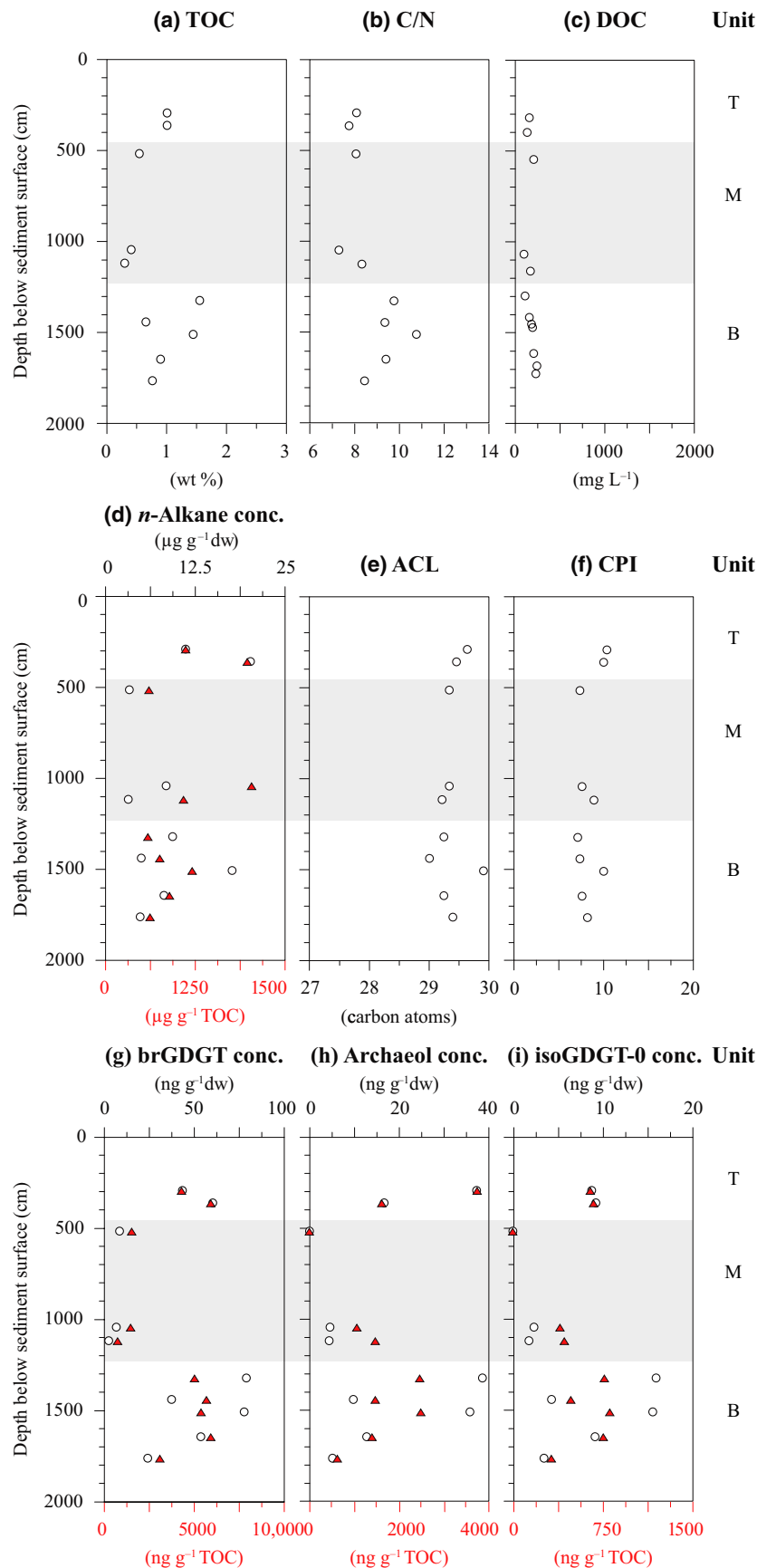#### 3.1.1 | Alas lake sediment core YU-L7

Core YU-L7 was divided into a bottom unit including sediments from 1769 to 1331 cm below the sediment surface (bss), a middle unit from 1125 to 518 cm bss and a top unit from 362 to 290 cm bss (Figure 3). This division was based on constrained hierarchical clustering of all measured parameters (Figure S3). The TOC ranged between 0.3 and 1.6 wt% (median: 0.8 wt%; Figure 3a) and was lowest in the middle unit. The C/N had a median of 8.3 and was highest in the bottom unit with the maximum of 10.7 at 1516 cm bss (Figure 3b). DOC values showed little variation and were between 97 and 242 mg L^{-1}

(median: 169 mg L^{-1}; Figure 3c). The *n*-alkane concentration per gram dry weight (g^{-1} dw) was highest at 362 cm bss with 20.1 μg g^{-1} dw and lowest at 518 cm bss with 3.1 μg g^{-1} dw (median: 8.24 μg g^{-1} dw; Figure 3d). The *n*-alkane concentration per gram TOC varied between 599 and 2048 μg and was especially high at 1048 and 362 cm bss (median: 993 μg g^{-1} TOC). The ACL showed little variation over depth between 29.0 and 29.9 (Figure 3e). Long chain (*n*-C_{29} and *n*-C_{31}) alkanes dominated all samples. The CPI ranged between 7.1 and 10.4 and did not show substantial variation between the units (Figure 3f). The brGDGT concentration ranged from 2.1 and 79.1 ng g^{-1} dw and was highest at 1516 and 1446 cm bss (median: 40.0 ng g^{-1} dw; Figure 3g). The brGDGT concentration per gram TOC varied between 2674 and 5455 ng (median: 2.9 μg g^{-1} TOC). The archaeol concentration showed quite some variation between 0 and 38.7 ng g^{-1} dw with relatively high values at 1331, 1516, and 290 cm bss (Figure 3h). Per gram TOC, the archaeol concentration was highest at 591 cm bss (3755 ng g^{-1}). The isoGDGT-0 concentration showed a similar pattern to the brGDGT concentration and ranged from 0 to 15.8 ng g^{-1} dw, and from 0 to 1084 ng g^{-1} TOC (Figure 3i). The results from the open-system pyrolysis (Figure 5) suggested a more aliphatic character for samples with higher TOC values (at 1331 cm bss, followed by 1561 and 362 cm bss). All results were published in the PANGAEA research data repository, specifically the biogeochemical parameters, *n*-alkane and brGDGT concentrations, cumulative GHG production, and DOC content (Jongejans et al., 2021a, 2021b, 2021c, 2021d, 2021e).

3.1.2 | Yedoma lake sediment core YU-L15

Core YU-L15 was divided into two parts: the bottom unit included the sediments from 1713 to 778 cm bss and the top unit from 353 to 170 cm bss (Figure 4; Figure S3). The TOC varied between 0.2 and 1.4 wt% (median: 0.5 wt%; Figure 4a). The TOC was slightly higher in the lowermost three samples (1713–1488 cm bss) and those at the top compared to the intermediate samples between 1315 and 778 cm bss. The C/N ratio had its maximum (13.2) as well as its minimum (8.9) in the top unit (Figure 4b). In the bottom unit, the C/N varied between 9.1 and 11.0 (core median: 9.7). The DOC concentration showed a lot of variation ranging from 51 to 1620 mg L^{-1} with highest concentrations at the base of the core (1694–1185 cm bss; median: 448 mg L^{-1}; Figure 4c). In the top unit of YU-L15, DOC values were between 437 and 615 mg L^{-1}. The *n*-alkane concentration was lowest in the upper sample at 170 cm bss (2.2 μg g^{-1} dw) and highest at 353 cm bss (median: 8.8 μg g^{-1} dw; Figure 4d). Per gram TOC, the *n*-alkane concentration was between 346 and 2456 μg and especially high between 1516 and 1076 cm bss. The ACL was higher than 28.8 in all samples (median: 29.0; Figure 4e). All samples were dominated by *n*-C_{29} and *n*-C_{31}. The CPI varied between 6.3 and 10.7 (Figure 4f). The brGDGT concentration was highest in the upper sample (58.7 ng g^{-1} dw) and lowest at 1315 cm bss (median: 7.9 ng g^{-1} dw; Figure 4g). The brGDGT concentration per gram TOC was up to 8744 ng g^{-1}. The archaeol (Figure 4h) and isoGDGT-0 concentration (Figure 4i) showed a very similar pattern with the highest

FIGURE 3 Biogeochemical parameters of Alas lake sediment core YU-L7. (a) Total organic carbon (TOC) content, (b) ratio of carbon to nitrogen content (C/N), (c) dissolved organic carbon (DOC) content of original pore water samples, (d) *n*-alkane concentration per gram dry weight (g^{-1} dw) and per gram TOC (orange triangles), (e) *n*-alkane average chain length, (f) *n*-alkane carbon preference index (CPI), (g) branched glycerol dialkyl glycerol tetraether (brGDGT) concentration g^{-1} dw and g^{-1} TOC (orange triangles), (h) archaeol concentration g^{-1} dw and g^{-1} TOC (orange triangles), and (i) isoGDGT-0 concentration g^{-1} dw and g^{-1} TOC (orange triangles). Units indicated on right: top (T), middle (M; gray area), and bottom (B)

concentration at 353 cm bss (26.1 and 6.1 ng g^{-1} dw, respectively) and a median of 2.8 and 1.1 ng g^{-1} dw, respectively. Per gram TOC, the maxima were 1861 and 433 ng g^{-1} for archaeol and isoGDGT-0,

respectively. Following pyrolysis, samples with the highest TOC values (353–1488 cm bss) are also among those with the highest aliphatic character (Figure 5).
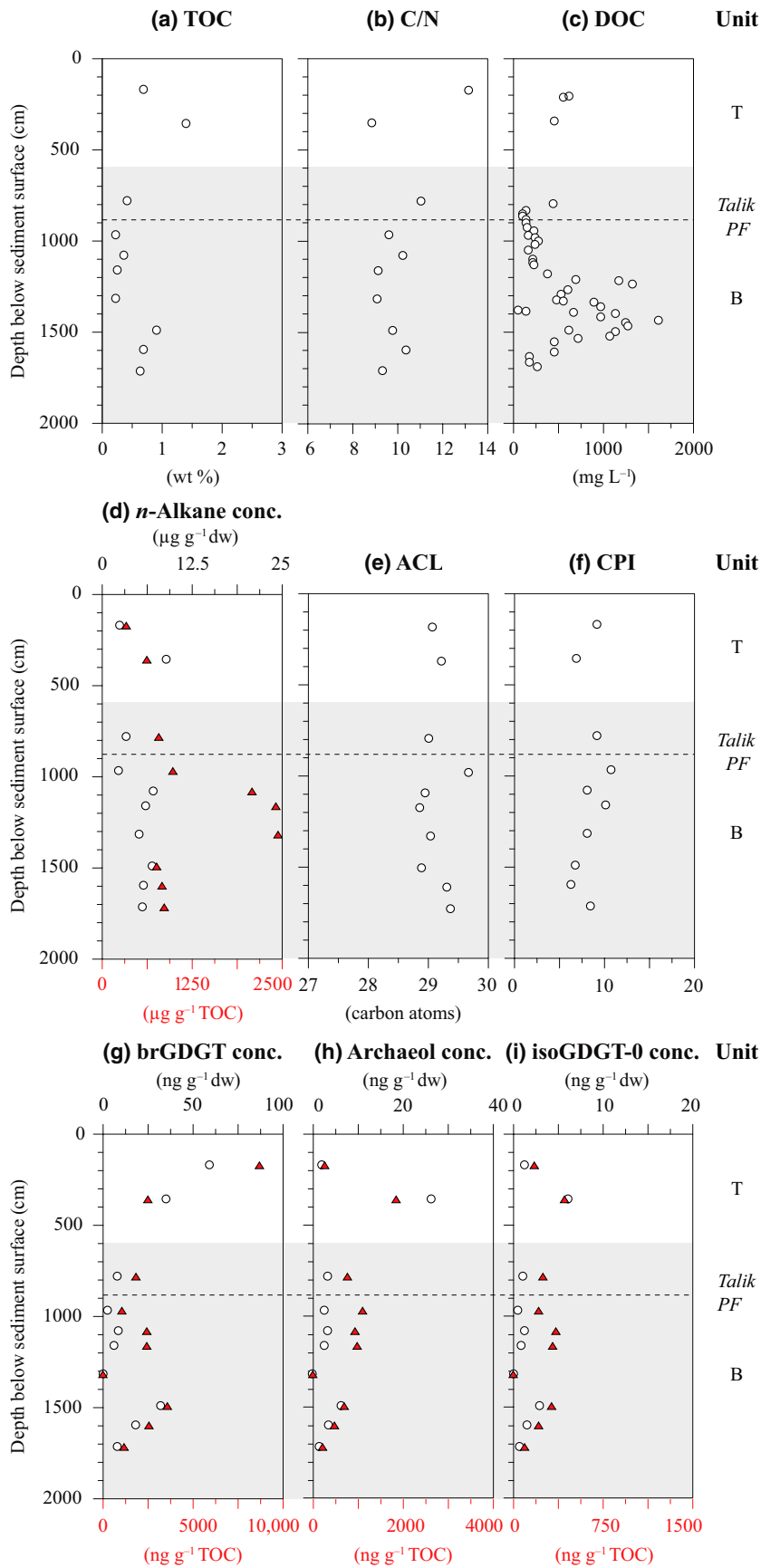
FIGURE 4 Biogeochemical parameters of Yedoma lake sediment core YU-L15. (a) Total organic carbon (TOC) content, (b) ratio of carbon to nitrogen content (C/N), (c) dissolved organic carbon (DOC) content of original pore water samples, (d) *n*-alkane concentration per gram dry weight (g⁻¹ dw) and per gram TOC (orange triangles), (e) *n*-alkane average chain length, (f) *n*-alkane carbon preference index (CPI), (g) branched glycerol dialkyl glycerol tetraether (brGDGT) concentration g⁻¹ dw and g⁻¹ TOC (orange triangles), (h) archaeol concentration g⁻¹ dw and g⁻¹ TOC (orange triangles), and (i) isoGDGT-0 concentration g⁻¹ dw and g⁻¹ TOC (orange triangles). Units indicated on right: top (T) and bottom (B; gray area), boundary talik to permafrost (PF) indicated with gray dashed line

3.2 | Greenhouse gas production

3.2.1 | Alas lake sediment core YU-L7

In total, we measured anaerobic GHG production of 10 samples from the Alas lake sediment core YU-L7 (Figure 6). CH_4 production after 1 year was highest (81.3 ± 38.2 µg CH_4-C g^{-1} dw; mean ± standard deviation) in the sample closest to the sediment surface in the top part at 290 cm bss (Figure 6a). Furthermore, CH_4 production also exceeded 20 µg for the sediments at 1048 cm (54.5 ± 42.7 µg CH_4-C g^{-1} dw) and 1769 cm bss (38.7 ± 66.3 µg CH_4-C g^{-1} dw). When normalized to gram TOC, CH_4 production was highest in the middle part of the core at 1048 cm bss (13.2 ± 10.4 mg CH_4-C g^{-1} TOC). There was no trend in depth observed. For the three samples with the highest CH_4 production, the maximum production rates
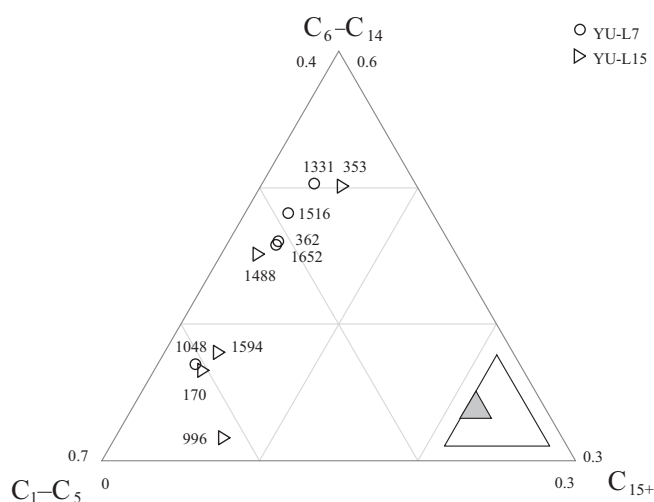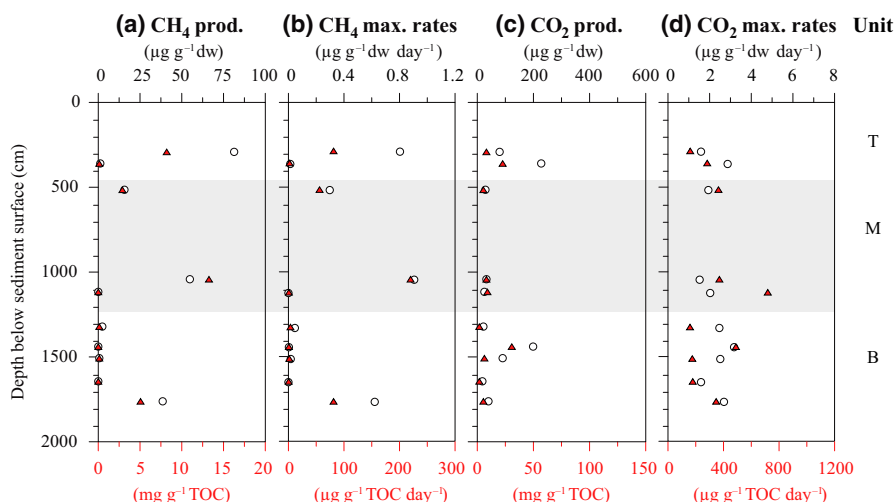
ranged from 0.62 to 0.91 µg CH_4-C g^{-1} dw day^{-1} (Figure 6b). After ~350 days, the rates of these samples decreased. In samples yielding higher CH_4 concentrations, CH_4 production started after ~200 days and increased exponentially. In 6 out of 10 samples, the CH_4 rates increased over time. Cumulative GHG production and rates for all replicates are shown in the supplement (Figures S6–S22).

CO_2 production was highest in the top part of the sediment core at 362 cm bss (227.15 ± 248.8 µg CO_2-C g^{-1} dw), closely followed by the sample at 1446 cm bss in the bottom unit (197.6 ± 225.7 µg CO_2-C g^{-1} dw; Figure 6c). In the middle unit, CO_2 production was very low. The CO_2 production per gram TOC was highest at 1446 cm bss (30.5 ± 34.8 mg CO_2-C g^{-1} TOC). In contrast to CH_4, CO_2 was produced from the start of the incubation and after which the rates decreased (e.g., Figure S6). Maximum rates of all samples varied between 1.52 and 3.17 µg CO_2-C g^{-1} dw day^{-1} (Figure 6d).

3.2.2 | Yedoma lake sediment core YU-L15

Anaerobic GHG production was measured on seven samples from the Yedoma lake sediment core YU-L15 (Figure 7). CH_4 production in the Yedoma lake sediment core YU-L15 was highest in the top of the core (Figure 7a). The maximum was at 353 cm bss with 87.0 ± 44.0 µg CH_4-C g^{-1} dw. The sample at 170 and 966 cm bss also showed substantial CH_4 production (64.1 ± 57.2 and 41.6 ± 26.9 µg CH_4-C g^{-1} dw, respectively). The CH_4 production normalized to gram TOC was highest in the sample at 966 cm bss (18.8 ± 12.2 mg CH_4-C g^{-1} TOC). Like in the Alas lake core, CH_4 production started after 200 days for most samples and increased exponentially (e.g., Figure S6). In five samples, the CH_4 production rates increased over time and were highest at the end of the incubations from 300 days and onward. The three samples with the highest cumulative CH_4 production (353, 170, and 966 cm bss) also had the highest rates ranging from 0.56 to 1.15 µg CH_4-C g^{-1} dw day^{-1} (Figure 7b).

The CO_2 production was highest in the bottom of the core (Figure 7c). The maximum CO_2 production was observed in the sample at 1488 cm bss (561.5 ± 527.4 µg CO_2-C g^{-1} dw). In the

FIGURE 5 Horsfield diagram: Chain length distribution of short (C_1–C_5), intermediate (C_6–C_{14}), and long (C_{15+}) n-alkanes and n-alk-1-enes after pyrolysis of the bitumen-free macromolecular organic matrix after Horsfield et al. (1989). Symbols correspond to samples from Alas lake sediment core YU-L7 (circles) and Yedoma lake sediment core YU-L15 (triangles)

FIGURE 6 Greenhouse gas production after 1 year from Alas lake sediment core YU-L7. (a) Cumulative methane (CH_4) production in per gram dry weight (g^{-1} dw; circles) and per gram TOC (orange triangles), (b) maximum CH_4 rates g^{-1} dw (circles) and g^{-1} TOC (orange triangles), (c) cumulative carbon dioxide (CO_2) production in g^{-1} dw (circles) and g^{-1} TOC (orange triangles), (d). maximum CO_2 rates g^{-1} dw (circles) and g^{-1} TOC (orange triangles). Units indicated on right: top (T), middle (M; gray area), and bottom (B)
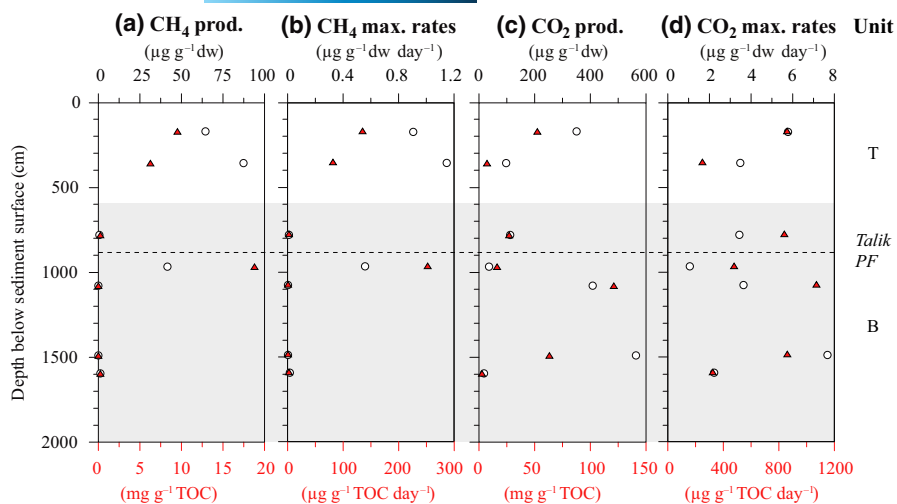
FIGURE 7 Greenhouse gas production after 1 year from Yedoma lake sediment core YU-L15. (a) Cumulative methane (CH_4) production in per gram dry weight (g^{-1} dw; circles) and per gram TOC (orange triangles), (b) maximum CH_4 rates g^{-1} dw (circles) and g^{-1} TOC (orange triangles), (c) cumulative carbon dioxide (CO_2) production in g^{-1} dw (circles) and g^{-1} TOC (orange triangles), (d) maximum CO_2 rates g^{-1} dw (circles) and g^{-1} TOC (orange triangles). Units indicated on right: top (T), middle (M; gray area), and bottom (B)

sample at 1076 cm (407.7 ± 680.1 µg CO_2-C g^{-1} dw) and 170 cm bss (350.2 ± 346.9 µg CO_2-C g^{-1} dw), CO_2 production was also high. All samples produced more than 50 µg CO_2-C, except for the sample at 1594 and 966 cm bss. The production per gram TOC was highest at 1076 cm bss (120.6 ± 201.2 mg CO_2-C g^{-1} TOC). CO_2 production started at the beginning of the incubation and increased gradually over time. Maximum CO_2 production rates ranged from 1.05 to 7.67 µg CO_2-C g^{-1} dw day^{-1} (Figure 7d).

3.2.3 | Carbon mineralization

Total anaerobic C production ranged from 0.02 to 0.23 mg g^{-1} dw in YU-L7 (max: 0.08 mg C g^{-1} dw as CH_4) and from 0.02 to 0.56 mg g^{-1} dw in YU-L15 (max: 0.09 mg C g^{-1} dw as CH_4). After 1 year, on average, 2.3 ± 3.1% of the initial carbon was mineralized to CO_2 and 0.4 ± 0.6% to CH_4 (Figure S4). In the first 100 days, 10 ± 21% of the cumulative CH_4 was produced. Production of CH_4 commenced after 200 days and CH_4 production rates were highest after 300 days in most samples. In six samples (YU-L7: 1125, 1446, and 1652 cm bss; YU-L15: 778, 1076 and 1488 cm bss; Figures S10, S12, S14, S18, S20, and S22), the CH_4 production was higher in the first week compared to the following weeks.

The CO_2 production rates were highest in the first 100 days in 8 out of 17 samples. In four samples, the rates were highest after 300 days. Within the first 100 days, 49 ± 28% of the cumulative CO_2 was produced. CO_2 production was generally highest at the beginning of the incubations and gradually decreased over time.

3.3 | Statistical correlation and regression

Considering both cores, the TOC correlated positively with n-alkane, brGDGT, archaeol, and isoGDGT-0 concentration ($p < 0.01$; Figure S5). The CO_2 production was correlated with the ACL (R: −0.56, $p < 0.05$) and with the DOC content in adjacent samples (R: 0.58,
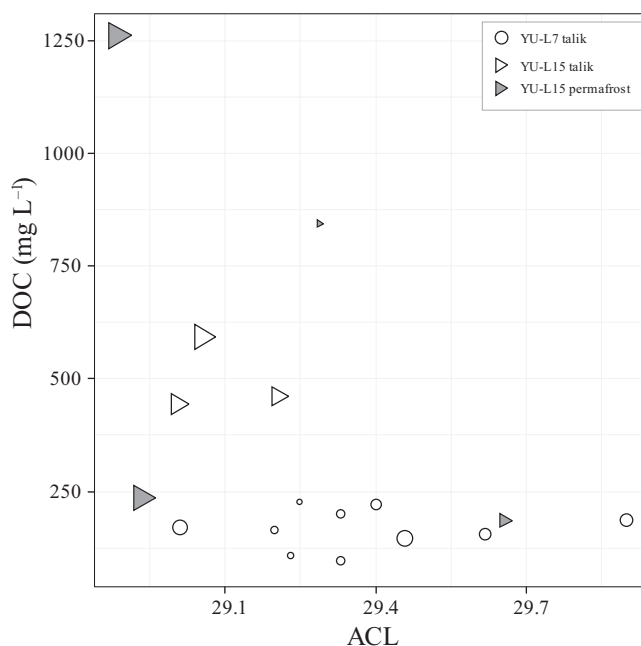
FIGURE 8 Bivariate scatterplot illustrates the relation of the n-alkane average chain length (ACL) and dissolved organic carbon (DOC) content with the cumulative carbon dioxide (CO_2) production after 1 year (indicated by symbol size). Samples from Alas lake sediment core (circles), talik of Yedoma lake sediment core (white triangles), and permafrost from Yedoma lake sediment core (gray triangles)

$p < 0.05$). The CH_4 production was negatively correlated with the depth (R: −0.58, $p < 0.05$).

Using the forward-selection stepwise multiple regression method, we found that the CH_4 production could not be explained by our data; no fitting model was found. The cumulative CO_2 production can be explained by a generalized linear regression model as shown in Equation (3). This model describes 73.5% of the variance of the cumulative CO_2 production, of which 58.5% is explained by the DOC content and the ACL alone. This clear relation of the CO_2 production with a high DOC and low ACL is also shown in Figure 8.

$$CO_2 = 0.27 \cdot DOC - 498.07 \cdot ACL + 60.92 \cdot CPI$$
$$+ 13.46 \cdot n\text{-alkane conc.} + 14{,}026.43. \qquad (3)$$

4 | DISCUSSION

4.1 | Organic matter degradation potential

4.1.1 | Organic carbon quantity

Sedimentary OC exists bound to the sediments or in the pore water. Total organic carbon (TOC) contains both the particulate (POC) and dissolved fractions of OC. In both Yukechi cores, the TOC was very low (median YU-L7: 0.8 wt% and median YU-L15: 0.5 wt%; Figures 3 and 4). Windirsch et al. (2020) found similar low values in sediment cores drilled on dry land within the same Alas basin (median: <0.1 wt%, max: 2.4 wt%) and on Yedoma upland nearby (median: <0.1 wt%, max: 1.7 wt%). They reported that the Yedoma sediments are rather coarse-grained (i.e., fine sand dominated) at the Yukechi study site compared to other Yedoma sites such as the Kolyma upland region, where Yedoma is dominated by fine-grained silt-sized grain fractions (Schirrmeister et al., 2020). OM in the mineral fraction is mainly bound to silt and clay (Mueller et al., 2015). Fluvial deposition of the Yukechi sands may explain the lack of OM (Windirsch et al., 2020). In contrast to our study site, Yedoma deposits in other regions of Siberia are characterized by finer grained silty sediments with relatively high TOC values with a median of 1.9 wt% (Strauss et al., 2012, 2020).

In contrast to the TOC, the DOC values from the frozen Yedoma sediments of YU-L15 are very high (median: 373 mg L^{-1}, max: 1620 mg L^{-1}; Figure 3), yet comparable to pore water from Yedoma deposits on Buor Khaya, northeastern Siberia (median: 317 mg L^{-1}, max: 1371 mg L^{-1}; Schirrmeister et al., 2017). In addition, Ewing et al. (2015) reported high maximum DOC values in Alaskan Yedoma pore water (median: 618 mg L^{-1}, max: 1551 mg L^{-1}). For comparison, other studies from northeastern Siberia reported much lower pore water DOC values such as for early to middle Weichselian sediments on the Cape Mamontov Klyk, ranging from 4 to 305 mg L^{-1} (Mitzscherling et al., 2019), or for Samoylov Island, ranging from 57 to 288 mg L^{-1} (Liebner et al., 2008).

The rate and efficiency of hydrolysis from POC to DOC as well as the size and quality of the DOC pool are of utmost importance for GHG production since microbes mainly metabolize DOC size fractions (Battin et al., 2008). Therefore, DOC in pore water is readily bioavailable for microbial degradation upon talik formation and hence a very important OM fraction in GHG production process. Recent studies showed that DOC from thawing permafrost is highly biodegradable with the biolabile fractions composing ~20%–53% for Alaskan sites (Drake et al., 2015; Ewing et al., 2015) and 34%–50% for Siberian sites (Spencer et al., 2015; Vonk et al., 2013). These studies found that the biolabile DOC fraction was lost mainly in the first 1–2 weeks upon thaw. Furthermore, it was shown that ancient DOC originating from Pleistocene permafrost was more susceptible to decomposition than modern DOC

(Mann et al., 2015; Vonk et al., 2013). The relatively high DOC contents in the Pleistocene Yedoma sediments in the bottom of core YU-L15 in combination with the generally high biolability of Yedoma OM could therefore be a reason for the substantial GHG production observed. The generally higher GHG production per gram TOC in contrast to unfrozen or Alas lake sediments (Figures 3 and 4) supports the relatively high bioavailability of Yedoma OM. Whereas the decomposition of labile DOC seems to contribute to the GHG production upon initial talik formation, GHG production at later stages of talik formation is primarily driven by the breakdown of the POC fraction. Only very few studies focus on the breakdown of POC, and the interaction between POC and DOC decomposition is not well understood. Nevertheless, it was shown that POC turnover is relevant for DOC decomposition (Attermeyer et al., 2018; Richardson et al., 2013).

4.1.2 | Organic matter preservation and talik formation

The characteristics of the sediments directly below alas lakes are often the result of several subsequent lake generations at a location with sometimes lacustrine and subaerial deposition alternating (Katasonov et al., 1979; Lenz et al., 2016; Soloviev, 1959). In many thermokarst lake regions, multiple thermokarst lake generations over the past centuries to millennia led to repeated thawing and refreezing of the sediments (e.g., Jones et al., 2012) and therefore likely also recurring talik formation (Grosse et al., 2013). For the Yukechi Alas, the domination of long-chain alkanes (n-C_{29} and n-C_{31}) throughout both cores, indicating OM from higher terrestrial plants, suggests that the Alas lake sediments are primarily thawed Yedoma sediments. However, dated macrofossils at 290 cm bss yielded a Holocene age (3.75 ± 0.12 cal kyr BP; Jongejans et al., 2019), suggesting a recent productivity signal in these sediments. The sediments at 518 cm bss had an age of 13.53 ± 0.66 cal kyr BP and all dated sediments below yielded ^{14}C ages >24 cal kyr BP.

In the uppermost sediments of the Yedoma lake core (170 cm bss), the OM is of recent origin (0.14 ± 0.05 cal kyr BP). This could be caused by sediment mixing during surface subsidence (Farquharson et al., 2016). Alternatively, active layer dynamics or cryoturbation could have played a role in the uppermost sediments during various sedimentation stages as well as the input of eroded material from the lakeshore. All other dated samples yielded ^{14}C ages >24 cal kyr BP. Hence, we measured GHG production from samples containing old and recent OM but found no clear pattern between the amount of GHG produced and the age of the OM. Nevertheless, the high and constant ACL over depth in both cores suggests that the OM source was rather similar over time.

With thaw and talik formation at our Alas site, microbial decomposition of OM led to GHG production. Furthermore, the drying of the basins could have favored aerobic conditions and OM cycling as well as potentially permafrost re-aggradation (Lee et al., 2012). This, in combination with the low TOC in the Yukechi Alas, could explain

the low DOC values in the Alas core. During phases of intensified lake formation, interactions between pore water and the mineral phase could have led to liberation of DOC and the microbial transformation of the most biolabile fraction into GHG.

The sediments underneath the Yedoma lake have been thawed from the top down only for the last ~70 years for the first time since deposition (Ulrich et al., 2017), explaining the rather shallow talik compared to the Alas lake. The sediments at 778 cm bss of the Yedoma lake core, which was part of the talik, were attributed to the bottom cluster. This suggests that the studied OM characteristics in this sample are still more similar to the frozen sediments underneath than to the talik sediments above.

The frozen sediments in the bottom part have likely not been thawed since permafrost formation in the late Pleistocene. This suggests OM was better preserved in the permafrost sediments of the Yedoma lake compared to the top of the Alas lake sediments (Schuur et al., 2009). This was corroborated by a higher C/N ratio in the Yedoma lake sediments and in the bottom of the Alas lake sediments compared to the top and middle of YU-L7 ($p < 0.05$; Figures 3 and 4). However, we found no significant correlation between the OC loss (Figure S4) and the C/N ratio. This might be the result of the low TOC content in the Yukechi sediments; consequently, TOC and C/N are no reliable predictors of CO_2 production. In the biomarker-based degradation indicators such as the $CPI_{n-alkanes}$, we did not see the better preservation signal of the OM in the Yedoma lake core compared to the Alas lake core (Figures 3 and 4). Potentially, not enough time has passed since deposition for maturation (Bray & Evans, 1961). The CPI must hence be a result of the original signal and depositional environment of the OM rather than permafrost thaw history (Jongejans et al., 2020).

Stapel et al. (2018) showed that the OM from Yedoma deposits on Bol'shoy Lyakhovsky Island had a relatively high aliphatic proportion, which suggests the OM is more easily degradable compared to more aromatic OM. Our pyrolysis experiments showed a clear connection between the TOC content and the aliphatic character, which suggests that these samples might contain more biolabile OM.

4.1.3 | Presence of methanogenic communities

Archaeol and isoGDGT-0 concentrations were significantly higher in the Alas compared to the Yedoma lake sediments ($p < 0.05$ and $p < 0.01$, respectively; Figures 3 and 4). Archaeol and isoGDGT-0 are breakdown products of intact polar membrane lipids and represent the past archaeal biomass as a degradation product (Bischoff et al., 2013; Stapel et al., 2018). Archaeol, one of the main core membrane lipids of archaea, was used to infer methanogenic abundance specifically before (Bischoff et al., 2013; Pancost et al., 2011). Increased isoGDGT-0 and archaeol concentrations in thawed sediments can indicate a mixture of past and present archaea including methanogens. The higher archaeal marker concentration in the Alas lake core suggests that the methanogenic communities were likely established after talik formation.

In previous studies, a positive correlation was found between CH_4 production in thawing permafrost and the presence of methanogenic archaea (Carnevali et al., 2015; Holm et al., 2020; Knoblauch et al., 2018). In our study, the CH_4 production was higher in the talik sediments of the Yedoma lake core. Lower CH_4 and CO_2 production in YU-L7 compared to YU-L15 suggests that the biolabile fraction of OM was already largely decomposed in a talik in previous thermokarst lake stages. This is corroborated by the lower C/N ratio in the Alas lake sediments. The moderate concentrations in the Yedoma lake core between 1161 and 966 cm bss might result from microbial activity during sedimentation (Bischoff et al., 2013). Holm et al. (2020) showed that microbial communities established prior to freezing could lead to an earlier start and stronger CH_4 production compared to sediments where no prior communities were established. Further research is needed to study the interactions between present and past microbial communities, and the factors controlling GHG production in thawing permafrost.

4.2 | Greenhouse gas production

The 1-year-long incubation experiments showed distinct differences between the first-generation and multiple-generation thermokarst lake sediments. Both CH_4 and CO_2 production were higher in the Yedoma lake sediments compared to the Alas lake sediments (3 and 1.5 times higher mean, respectively). The GHG production did neither correlate with the TOC content nor with the biomarker concentrations and indices. Previous incubation studies of permafrost sediments found a positive correlation between CO_2 production and TOC (Knoblauch et al., 2013; Lee et al., 2012; Walter Anthony et al., 2016). These studies, however, analyzed sediment samples with higher TOC contents compared to our study (median: 1.2, 5.0, and ~4 wt%, respectively). Furthermore, we compared sediment samples that have undergone different depositional conditions and thaw legacy, which might explain the lack of correlation between TOC content and GHG production.

4.2.1 | Carbon dioxide production

CO_2 production was highest in the bottom of YU-L15 (Figure 4). This is likely because the sediments were thawed for the first time since deposition, and the presence of readily bioavailable DOC after thaw. The latter is corroborated by the positive correlation between the initial DOC values in samples adjacent to the incubation samples and the CO_2 production, supporting the rapid turnover of biolabile DOC fractions (Vonk et al., 2013). The CO_2 production from the still frozen Yedoma sediments in our core (1713–996 cm bss) is in the same order of magnitude as from Pleistocene sediments in the Lena Delta (0.13 ± 0.06 mg CO_2-C g^{-1} dw; Knoblauch et al., 2013) and from mineral soils in Alaska and Siberia (0.34 ± 0.13 mg CO_2-C g^{-1} dw; Lee et al., 2012). When expressed on a bulk carbon basis, however, the CO_2 production in the permafrost sediments of the Yedoma lake

(50.6 ± 53.4 mg CO_2-C g^{-1} TOC) is much higher than from other Yedoma sites as reported by Knoblauch et al. (2013; 4.9 ± 2.1 mg CO_2-C g^{-1} TOC) and Lee et al. (2012; 11.3 ± 12.3 mg CO_2-C g^{-1} TOC). This means that despite the low carbon content of these sediments, the overall mineral OM has a high potential for being degraded into CO_2. Nevertheless, the percentage of initial C that was mineralized to CO_2 (2.3 ± 3.1%) was low in comparison with -year-long incubation studies of organic-rich active layer sediments such as reported by Schädel et al. (2014; 6% loss) and Faucherre et al. (2018; 8% loss).

The median CO_2 rates over time in the bottom unit of the Yedoma lake core was 50 µg CO_2-C g^{-1} TOC day^{-1}. While some anaerobic incubations studies with permafrost samples had much lower CO_2 production rates (median: 1.6–3.6 µg CO_2-C g^{-1} TOC day^{-1}; Knoblauch et al., 2013; Zona et al., 2012), other studies found rates in the same order of magnitude as our data such as Lupascu et al. (2012) and Santruckova et al. (unpublished data; median 37.8 and 68.6 µg CO_2-C g^{-1} TOC day^{-1}, respectively). However, of these studies, only Knoblauch et al. (2013) reported CO_2 production in sediments >1 m bss (i.e., down to 25 m depth).

The relatively high GHG production at the uppermost sample (290 cm bss) of the Alas lake sediment core might be explained by the input of Holocene OM (see Section 4.1.2) during a previous thermokarst lake stage where methanogenic communities were established, which might have a priming effect on the older carbon in these sediments (Wild et al., 2014).

4.2.2 | Methane production

In most of our samples, a significant start of CH_4 production could be recognized only after 200 days (Figures S5 and S6). Previous incubation studies also observed this lag phase and explained it as the result of the low initial abundance of methanogens in the sediments, which increases with thaw (Knoblauch et al., 2013, 2018; Treat et al., 2014; Waldrop et al., 2010). Interestingly, the frozen sample below the talik boundary in the Yedoma lake core (996 cm bss), showed the highest maximum CH_4 production rate (252.2 µg CH_4-C g^{-1} TOC day^{-1}). As these sediments were frozen continuously since deposition and permafrost incorporation, these findings suggest that methanogenic communities were established here prior or during deposition and survived while being freeze-locked (Holm et al., 2020). In this particular sample, methanogenic taxa were likely present that produce CH_4 using very low substrate TOC concentrations as reported from low-temperature incubations of Arctic soils (Blake et al., 2015), but further detailed microbial analyses are required to substantiate this hypothesis.

CH_4 production was highest in the top of Yedoma lake core (Figure 7), which is corroborated by a negative correlation between CH_4 production and the depth bss in this core. This fits well to thaw front migration with talik formation and subsequent gradual population of methanogenic communities. In their study of methanogenesis response to permafrost thaw, Holm et al. (2020) found that CH_4 production was not correlated to C content, but rather to

paleoenvironmental conditions. They argued that CH_4 production is more vulnerable to disturbance than anoxic CO_2 production, because methanogenesis is restricted to a very small group of archaea whereas there are many different groups of microorganisms producing CO_2 under anoxic conditions. Their findings show that anaerobic GHG release from thawing permafrost is complex and not yet well understood.

To our knowledge, Heslop et al. (2015) present the only other CH_4 production rates from Yedoma deposits that were thawed in a talik. They measured C release rates as CH_4 along a talik profile below an Alaskan first-generation thermokarst lake. In contrast to our data, Heslop et al. (2015) found highest CH_4 production rates in the recently thawed sediments (59.6 ± 51.5 µg CH_4-C g^{-1} TOC day^{-1}) compared to the transitional permafrost (15.3 ± 9.1 µg CH_4-C g^{-1} TOC day^{-1}) and the thawed Yedoma sediments (17.9 ± 13.6 µg CH_4-C g^{-1} TOC day^{-1}). Our data did not show such a trend: sediments from the recently thawed permafrost (778 cm bss) had a low maximum CH_4 production rate (2.5 µg CH_4-C g^{-1} TOC day^{-1}). However, the rates from the top of YU-L15 (81.8–135.1 µg CH_4-C g^{-1} TOC day^{-1}) were much higher. Nevertheless, the CH_4 production is not necessarily directly linked to CH_4 release, since a part of the produced CH_4 might be oxidized in the sediment column before being released into the atmosphere (Winkel et al., 2019).

The CH_4 production rates in the bottom unit of the Yedoma lake core (median: 0.02 µg CH_4-C g^{-1} TOC day^{-1}) were much lower compared to previously published CH_4 rates in 4°C permafrost incubation studies (0.12–0.56 µg CH_4-C g^{-1} TOC day^{-1}; Knoblauch et al., 2013; Lupascu et al., 2012; Santruckova et al., unpublished data; Zona et al., 2012).

4.3 | GHG links with other parameters and outlook

Using the generalized linear regression models, we found that CO_2 production was mainly explained by the ACL and the DOC content: sediments with the lowest ACL and highest DOC content produced the most CO_2 (Figure 8). This suggests that these parameters describe the lability of the OM best for our study. While the DOC seems to indicate the abundance of bioavailable OM (see Section 4.1), the ACL signal might represent a more labile OM source fraction from the respective surrounding ecosystem.

In some cases, we did find high archaeal markers or a strong aliphatic character corresponding to a higher CH_4 production, but in other samples, this was the exact opposite. We did not find significant correlations between biomarker distribution and CH_4 production (Figure S5). Therefore, we assume that the variation must be explained by a complex interplay of different external factors controlling GHG production. The varying sedimentation history of the Yukechi sediments might play an important role in this, as different depositional mechanisms could have resulted in OM from different sources (e.g., transported vs. in situ, different types of plants) leading to a mixture of labile and recalcitrant OM. This could have led to an activation of OM in some (sub-)samples but not in others. For the

samples with increased bacterial and archaeal markers but low GHG production, the biomarkers might indicate past microbial activity rather than the presence of active methanogenic communities. The reactivation of such paleo-active horizons depends on factors which are not yet fully understood, but intense remineralization in the past as indicated by the high lipid biomarker concentrations might have strongly depleted labile organic compounds from the overall OM pool. Further research into intact polar lipids could help to quantify the interaction between present and past microorganisms (Bischoff et al., 2013; Stapel et al., 2018).

In contrast to our incubation experiment, external factors could influence the oxygen content of the sediments as well as the soil microbial communities under in situ conditions. Differences between the temperature used in our incubations (4°C) and the actual temperature in talik sediments, which varies seasonally depending on the depth and probably ranges from ~0°C to about 4°C (Heslop et al., 2015), might lead to over- or underestimation of GHG production. Earlier incubations (e.g., Tanski et al., 2019) and modeling research (e.g., Knoblauch et al., 2013) considered GHG production for 4 months per year, which represents the summer thaw season. GHG production in talik sediments, however, continues year-round, which is why we incubated our samples for one entire year.

Thermokarst lake initiation and expansion in a warming climate will continue to set free OM. Even though initially microbial abundances might be low in permafrost soils, long-term thawing of ice-rich sediments underneath thermokarst lakes will promote anaerobic conditions and activate methanogenic OM degradation, leading to substantial GHG production. Walter Anthony et al. (2016) showed that anaerobic carbon release from thermokarst lakes was directly proportional to the amount of carbon input by thawing of sediments. They calculated that, since the 1950s, 0.2–2.5 Gt permafrost carbon was released as GHG in thermokarst expansion zones of pan-Arctic lakes. Converted to annual release, they found a mean CH_4 production of 0.50 ± 0.09 mg CH_4-C g^{-1} TOC year^{-1}, which is much lower than the mean of all our samples after 1 year (3.80 ± 5.66 mg CH_4-C g^{-1} TOC). Our findings underline the vast potential of thermokarst lake formation and subsequent GHG release. Considering the importance of this input for the global climate system, this topic should receive continued attention.

5 | CONCLUSION

In this study, we analyzed GHG production and lipid biomarker distributions in two 17-m-long thermokarst lake sediment cores taken in Central Yakutia, Russia. We found that the sediments in both cores were relatively OC poor, which is in agreement with previous research in the Yukechi region. We found substantial differences between the well-preserved sediments below a young Yedoma lake, and the heavily thermokarst-affected sediments below an Alas lake. Both CH_4 and CO_2 production were higher in the Yedoma lake deposits compared to Alas lake deposits. The highest CO_2 production

was measured in the deepest, in situ still frozen part of the Yedoma lake core, which shows that potential CO_2 production in newly thawed sediments strongly depends on the decomposition of readily available DOC. In contrast to previous research, we found no correlation between CO_2 production and TOC content. However, CO_2 production could mainly be explained by the ACL and DOC content, suggesting that OM source and quality is the main driver for CO_2 production. CH_4 production showed a different pattern: most CH_4 was produced in the talik sediments below the Yedoma lake, suggesting that methanogenic communities were established in the thawed sediments but not yet in the frozen sediments in the bottom of the core. We assume that the variable depositional history of the Yukechi region led to the accumulation of OM from a different source and quality in different sediment layers, which explains the variation in GHG production in the sediments. The lower GHG production in the Alas lake core is a result of a degradation legacy that led to OM decomposition during earlier thermokarst lake generations. GHG production from thawed permafrost was substantial even from OC-poor sediments, highlighting the importance of thermokarst formation in general, and thaw of mineral permafrost in particular for the climate system. Therefore, our study presents novel insights that are relevant for mineral-dominated deposits with generally low TOC contents, which are widespread throughout the Arctic.

CONFLICT OF INTEREST
The authors declare that there is no conflict of interest.

AUTHOR CONTRIBUTIONS
Loeka L. Jongejans wrote the initial draft of the manuscript. Loeka L. Jongejans and Jens Strauss designed the lab studies. Guido Grosse, Mathias Ulrich, Jens Strauss, Alexander N. Fedorov, and Pavel Ya. Konstantinov selected the field sites and conducted the drilling expedition. Loeka L. Jongejans, Susanne Liebner, and Christian Knoblauch conducted the incubation experiments. Loeka L. Jongejans and Kai Mangelsdorf carried out the lipid biomarker analysis. All authors contributed to the manuscript drafts and to manuscript finalization.

DATA AVAILABILITY STATEMENT

All results were published in the PANGAEA research data repository, specifically the biogeochemical parameters, *n*-alkane and brGDGT concentrations, cumulative GHG production, and DOC content (Jongejans et al., 2021a, 2021b, 2021c, 2021d, 2021e). The supplement includes additional images and tables illustrating the methods and results, including graphs of the GHG of all replicates.

ORCID

Loeka L. Jongejans https://orcid.org/0000-0002-0383-4567
Susanne Liebner https://orcid.org/0000-0002-9389-7093
Christian Knoblauch https://orcid.org/0000-0002-7147-1008
Mathias Ulrich https://orcid.org/0000-0002-1337-252X
Guido Grosse https://orcid.org/0000-0001-5895-2141
George Tanski https://orcid.org/0000-0002-2992-2071
Alexander N. Fedorov https://orcid.org/0000-0002-4016-2149
Torben Windirsch https://orcid.org/0000-0002-4292-6931
Jens Strauss https://orcid.org/0000-0003-4678-4982

REFERENCES

Attermeyer, K., Catalán, N., Einarsdóttir, K., Freixa, A., Groeneveld, M., Hawkes, J., Bergquist, J., & Tranvik, L. (2018). Organic carbon processing during transport through boreal inland waters: Particles as important sites. *Journal of Geophysical Research: Biogeosciences*, *123*, 2412–2428. https://doi.org/10.1029/2018JG004500

Battin, T. J., Kaplan, L. A., Findlay, S., Hopkinson, C. S., Marti, E., Packman, A. I., Newbold, J. D., & Sabater, F. (2008). Biophysical controls on organic carbon fluxes in fluvial networks. *Nature Geoscience*, *1*(2), 95–100. https://doi.org/10.1038/ngeo101

Bischoff, J., Mangelsdorf, K., Gattinger, A., Schloter, M., Kurchatova, A. N., Herzschuh, U., & Wagner, D. (2013). Response of methanogenic archaea to Late Pleistocene and Holocene climate changes in the Siberian Arctic: Methanogenic Response to Climate Changes. *Global Biogeochemical Cycles*, *27*(2), 305–317. https://doi.org/10.1029/2011GB004238

Biskaborn, B. K., Smith, S. L., Noetzli, J., Matthes, H., Vieira, G., Streletskiy, D. A., Schoeneich, P., Romanovsky, V. E., Lewkowicz, A. G., Abramov, A., Allard, M., Boike, J., Cable, W. L., Christiansen, H. H., Delaloye, R., Diekmann, B., Drozdov, D., Etzelmüller, B., Grosse, G., … Lantuit, H. (2019). Permafrost is warming at a global scale. *Nature Communications*, *10*(1), 264. https://doi.org/10.1038/s41467-018-08240-4

Blake, L. I., Tveit, A., Øvreås, L., Head, I. M., & Gray, N. D. (2015). Response of methanogens in arctic sediments to temperature and methanogenic substrate availability. *PLoS One*, *10*(6), e0129733. https://doi.org/10.1371/journal.pone.0129733

Bray, E. E., & Evans, E. D. (1961). Distribution of *n*-paraffins as a clue to recognition of source beds. *Geochimica et Cosmochimica Acta*, *22*(1), 2–15. https://doi.org/10.1016/0016-7037(61)90069-2

Čapek, P., Diáková, K., Dickopp, J.-E., Bárta, J., Wild, B., Schnecker, J., Alves, R. J. E., Aiglsdorfer, S., Guggenberger, G., Gentsch, N., Hugelius, G., Lashchinsky, N., Gittel, A., Schleper, C., Mikutta, R., Palmtag, J., Shibistova, O., Urich, T., Richter, A., & Šantrůčková, H. (2015). The effect of warming on the vulnerability of subducted organic carbon in arctic soils. *Soil Biology and Biochemistry*, *90*, 19–29. https://doi.org/10.1016/j.soilbio.2015.07.013

Carnevali, P. B. M., Rohrssen, M., Williams, M. R., Michaud, A. B., Adams, H., Berisford, D., Love, G. D., Priscu, J. C., Rassuchine, O., Hand, K. P., & Murray, A. E. (2015). Methane sources in arctic thermokarst lake sediments on the North Slope of Alaska. *Geobiology*, *13*(2), 181–197. https://doi.org/10.1111/gbi.12124

Climate-data.org. (2020, April). *Climate data for cities worldwide*. http://en.climate-data.org

Dean, J. F., Middelburg, J. J., Röckmann, T., Aerts, R., Blauw, L. G., Egger, M., Jetten, M. S. M., de Jong, A. E. E., Meisel, O. H., Rasigraf, O., Slomp, C. P., Zandt, M. H., in't Zandt, M. H., & Dolman, A. J. (2018). Methane feedbacks to the global climate system in a warmer world. *Reviews of Geophysics*, *56*(1), 207–250. https://doi.org/10.1002/2017RG000559

Diáková, K., Čapek, P., Kohoutová, I., Mpamah, P. A., Bárta, J., Biasi, C., Martikainen, P. J., & Šantrůčková, H. (2016). Heterogeneity of carbon loss and its temperature sensitivity in East-European subarctic tundra soils. *FEMS Microbiology Ecology*, *92*(9). https://doi.org/10.1093/femsec/fiw140

Drake, T. W., Wickland, K. P., Spencer, R. G. M., McKnight, D. M., & Striegl, R. G. (2015). Ancient low–molecular-weight organic acids in permafrost fuel rapid carbon dioxide production upon thaw. *Proceedings of the National Academy of Sciences of the United States of America*, *112*(45), 13946–13951. https://doi.org/10.1073/pnas.1511705112

Dutta, K., Schuur, E. A. G., Neff, J. C., & Zimov, S. A. (2006). Potential carbon release from permafrost soils of Northeastern Siberia. *Global Change Biology*, *12*(12), 2336–2351. https://doi.org/10.1111/j.1365-2486.2006.01259.x

Elberling, B., Michelsen, A., Schädel, C., Schuur, E. A. G., Christiansen, H. H., Berg, L., Tamstorf, M. P., & Sigsgaard, C. (2013). Long-term CO_2 production following permafrost thaw. *Nature Climate Change*, *3*(10), 890–894. https://doi.org/10.1038/nclimate1955

Estop-Aragonés, C., & Blodau, C. (2012). Effects of experimental drying intensity and duration on respiration and methane production recovery in fen peat incubations. *Soil Biology and Biochemistry*, *47*, 1–9. https://doi.org/10.1016/j.soilbio.2011.12.008

Ewing, S. A., O'Donnell, J. A., Aiken, G. R., Butler, K., Butman, D., Windham-Myers, L., & Kanevskiy, M. Z. (2015). Long-term anoxia and release of ancient, labile carbon upon thaw of Pleistocene permafrost. *Geophysical Research Letters*, *42*(24), https://doi.org/10.1002/2015GL066296

Farquharson, L., Anthony, K. W., Bigelow, N., Edwards, M., & Grosse, G. (2016). Facies analysis of yedoma thermokarst lakes on the northern Seward Peninsula, Alaska. *Sedimentary Geology*, *340*, 25–37. https://doi.org/10.1016/j.sedgeo.2016.01.002

Faucherre, S., Jørgensen, C. J., Blok, D., Weiss, N., Siewert, M. B., Bang-Andreasen, T., Hugelius, G., Kuhry, P., & Elberling, B. (2018). Short and long-term controls on active layer and permafrost carbon turnover across the arctic. *Journal of Geophysical Research: Biogeosciences*, *123*(2), 372–390. https://doi.org/10.1002/2017JG004069

Fedorov, A. N., Gavriliev, P. P., Konstantinov, P. Y., Hiyama, T., Iijima, Y., & Iwahana, G. (2014). Estimating the water balance of a thermokarst lake in the middle of the Lena River basin, eastern Siberia. *Ecohydrology*, *7*(2), 188–196. https://doi.org/10.1002/eco.1378

Fedorov, A. N., & Konstantinov, P. (2003). Observations of surface dynamics with thermokarst initiation, Yukechi site, Central Yakutia. *Proceedings of the 8th International Conference on Permafrost*, 21–25 July 2003, Zurich, Switzerland, 239–243.

Ficken, K. J., Barber, K. E., & Eglinton, G. (1998). Lipid biomarker, δ^{13}C and plant macrofossil stratigraphy of a Scottish montane peat bog over the last two millennia. *Organic Geochemistry*, *28*(3), 217–237. https://doi.org/10.1016/S0146-6380(97)00126-5

Groemping, U. (2006). Relative importance for linear regression in R: The package relaimpo. *Journal of Statistical Software, Articles*, *17*(1), 1–27. https://doi.org/10.18637/jss.v017.i01

Grosse, G., Harden, J., Turetsky, M., McGuire, A. D., Camill, P., Tarnocai, C., Frolking, S., Schuur, E. A. G., Jorgenson, T., Marchenko, S., Romanovsky, V., Wickland, K. P., French, N., Waldrop, M., Bourgeau-Chavez, L., & Striegl, R. G. (2011). Vulnerability of

high-latitude soil organic carbon in North America to disturbance. *Journal of Geophysical Research Biogeosciences*, 116(G4). https://doi.org/10.1029/2010JG001507

Grosse, G., Jones, B., & Arp, C. (2013). *8.21 Thermokarst lakes, drainage, and drained basins* (pp. 325–353).

Gundelwein, A., Müller-Lupp, T., Sommerkorn, M., Haupt, E. T. K., Pfeiffer, E.-M., & Wiechmann, H. (2007). Carbon in tundra soils in the Lake Labaz region of arctic Siberia. *European Journal of Soil Science*, 58(5), 1164–1174. https://doi.org/10.1111/j.1365-2389.2007.00908.x

Heslop, J. K., Anthony, K. M. W., Grosse, G., Liebner, S., & Winkel, M. (2019). Century-scale time since permafrost thaw affects temperature sensitivity of net methane production in thermokarst-lake and talik sediments. *Science of the Total Environment*, 691, 124–134. https://doi.org/10.1016/j.scitotenv.2019.06.402

Heslop, J. K., Walter Anthony, K. M., Sepulveda-Jauregui, A., Martinez-Cruz, K., Bondurant, A., Grosse, G., & Jones, M. C. (2015). Thermokarst lake methanogenesis along a complete talik profile. *Biogeosciences*, 12(14), 4317–4331. https://doi.org/10.5194/bg-12-4317-2015

Holm, S., Walz, J., Horn, F., Yang, S., Grigoriev, M. N., Wagner, D., Knoblauch, C., & Liebner, S. (2020). Methanogenic response to long-term permafrost thaw is determined by paleoenvironment. *FEMS Microbiology Ecology*, 96(3), fiaa021. https://doi.org/10.1093/femsec/fiaa021

Horsfield, B., Disko, U., & Leistner, F. (1989). The micro-scale simulation of maturation: Outline of a new technique and its potential applications. *Geologische Rundschau*, 78, 361–373. https://doi.org/10.1007/BF01988370

Jones, M. C., Grosse, G., Jones, B. M., & Walter Anthony, K. (2012). Peat accumulation in drained thermokarst lake basins in continuous, ice-rich permafrost, northern Seward Peninsula, Alaska. *Journal of Geophysical Research Biogeosciences*, 117(G2). https://doi.org/10.1029/2011JG001766

Jongejans, L. L., Grosse, G., Ulrich, M., Fedorov, A. N., Konstantinov, P., & Strauss, J. (2019). *Radiocarbon ages of talik sediments of an alas lake and a yedoma lake in the Yukechi Alas*. PANGAEA. https://doi.org/10.1594/PANGAEA.904738

Jongejans, L. L., Liebner, S., Knoblauch, C., Mangelsdorf, K., & Strauss, J. (2021a). Biogeochemical parameters of thawed sediments underneath a Yedoma and Alas thermokarst lake in Eastern Siberia. *PANGAEA*, https://doi.org/10.1594/PANGAEA.928132

Jongejans, L. L., Liebner, S., Knoblauch, C., Mangelsdorf, K., & Strauss, J. (2021b). Branched glycerol dialkyl glycerol tetraether (brGDGT) concentration in thawed sediments underneath a Yedoma and Alas thermokarst lake in Eastern Siberia. *PANGAEA*. https://doi.org/10.1594/PANGAEA.928135

Jongejans, L. L., Liebner, S., Knoblauch, C., Mangelsdorf, K., & Strauss, J. (2021c). Cumulative greenhouse gas production in thawed sediments underneath a Yedoma and Alas thermokarst lake in Eastern Siberia. *PANGAEA*. https://doi.org/10.1594/PANGAEA.928140

Jongejans, L. L., Liebner, S., Knoblauch, C., Mangelsdorf, K., & Strauss, J. (2021d). Dissolved organic carbon content in thawed sediments underneath a Yedoma and Alas thermokarst lake in Eastern Siberia. *PANGAEA*. https://doi.org/10.1594/PANGAEA.928136

Jongejans, L. L., Liebner, S., Knoblauch, C., Mangelsdorf, K., & Strauss, J. (2021e). n-Alkane concentration in thawed sediments underneath a Yedoma and Alas thermokarst lake in Eastern Siberia. *PANGAEA*. https://doi.org/10.1594/PANGAEA.928134

Jongejans, L. L., Mangelsdorf, K., Schirrmeister, L., Grigoriev, M. N., Maksimov, G. M., Biskaborn, B. K., Grosse, G., & Strauss, J. (2020). *n*-Alkane characteristics of thawed permafrost deposits below a Thermokarst Lake on Bykovsky Peninsula, Northeastern Siberia. *Frontiers in Environmental Science*, 8, 118. https://doi.org/10.3389/fenvs.2020.00118

Jongejans, L. L., Strauss, J., Lenz, J., Peterse, F., Mangelsdorf, K., Fuchs, M., & Grosse, G. (2018). Organic matter characteristics in yedoma and thermokarst deposits on Baldwin Peninsula, west Alaska. *Biogeosciences*, 15(20), 6033–6048. https://doi.org/10.5194/bg-15-6033-2018

Juggins, S. (2020). *rioja: Analysis of quaternary science data*. https://cran.r-project.org/package=rioja

Katasonov, E., Ivanov, M., & Pudov, G. (1979). Structure and absolute geochronology of alas deposits in Central Yakutia. *Novosibirsk: Science*, 95.

Killops, S. D., & Killops, V. J. (2013). 5.1.2 General differences between major groups of organisms. *Introduction to organic geochemistry* (p. 167). John Wiley & Sons. https://www.worldcat.org/title/introduction-to-organic-geochemistry/oclc/894718224&referer=brief_results

Knoblauch, C., Beer, C., Liebner, S., Grigoriev, M. N., & Pfeiffer, E.-M. (2018). Methane production as key to the greenhouse gas budget of thawing permafrost. *Nature Climate Change*, 8(4), 309–312. https://doi.org/10.1038/s41558-018-0095-z

Knoblauch, C., Beer, C., Sosnin, A., Wagner, D., & Pfeiffer, E.-M. (2013). Predicting long-term carbon mineralization and trace gas production from thawing permafrost of Northeast Siberia. *Global Change Biology*, 19(4), 1160–1172. https://doi.org/10.1111/gcb.12116

Kuhry, P., Bárta, J., Blok, D., Elberling, B., Faucherre, S., Hugelius, G., Jørgensen, C. J., Richter, A., Šantrůčková, H., & Weiss, N. (2020). Lability classification of soil organic matter in the northern permafrost region. *Biogeosciences*, 17(2), 361–379. https://doi.org/10.5194/bg-17-361-2020

Lee, H., Schuur, E. A. G., Inglett, K. S., Lavoie, M., & Chanton, J. P. (2012). The rate of permafrost carbon release under aerobic and anaerobic conditions and its potential effects on climate. *Global Change Biology*, 18(2), 515–527. https://doi.org/10.1111/j.1365-2486.2011.02519.x

Lenz, J., Wetterich, S., Jones, B. M., Meyer, H., Bobrov, A., & Grosse, G. (2016). Evidence of multiple thermokarst lake generations from an 11 800-year-old permafrost core on the northern Seward Peninsula. *Alaska. Boreas*, 45(4), 584–603. https://doi.org/10.1111/bor.12186

Liebner, S., Harder, J., & Wagner, D. (2008). Bacterial diversity and community structure in polygonal tundra soils from Samoylov Island, Lena Delta, Siberia. *International Microbiology*, 11, 195–202. https://doi.org/10.2436/20.1501.01.60

Lupascu, M., Wadham, J. L., Hornibrook, E. R. C., & Pancost, R. D. (2012). Temperature sensitivity of methane production in the permafrost active layer at Stordalen, Sweden: A comparison with non-permafrost northern wetlands. *Arctic, Antarctic, and Alpine Research*, 44(4), 469–482. https://doi.org/10.1657/1938-4246-44.4.469

Mann, P. J., Eglinton, T. I., McIntyre, C. P., Zimov, N., Davydova, A., Vonk, J. E., Holmes, R. M., & Spencer, R. G. M. (2015). Utilization of ancient permafrost carbon in headwaters of Arctic fluvial networks. *Nature Communications*, 6, 7856.

Marzi, R., Torkelson, B. E., & Olson, R. K. (1993). A revised carbon preference index. *Organic Geochemistry*, 20(8), 1303–1306. https://doi.org/10.1016/0146-6380(93)90016-5

Mitzscherling, J., Horn, F., Winterfeld, M., Mahler, L., Kallmeyer, J., Overduin, P. P., Schirrmeister, L., Winkel, M., Grigoriev, M. N., Wagner, D., & Liebner, S. (2019). Microbial community composition and abundance after millennia of submarine permafrost warming. *Biogeosciences*, 16(19), 3941–3958. https://doi.org/10.5194/bg-16-3941-2019

Mueller, C. W., Rethemeyer, J., Kao-Kniffin, J., Löppmann, S., Hinkel, K. M., & G. Bockheim, J. (2015). Large amounts of labile organic carbon in permafrost soils of northern Alaska. *Global Change Biology*, 21(7), 2804–2817. https://doi.org/10.1111/gcb.12876

Myhre, G., Shindell, D., Bréon, F.-M., Collins, W., Fuglestvedt, J., Huang, J., Koch, D., Lamarque, J.-F., Lee, D., Mendoza, B., Nakajima, T., Robock, A., Stephens, G., Takemura, T., & Zhang,

H. (2013). Anthropogenic and natural radiative forcing. In T. F. Stocker, D. Qin, G.-K. Plattner, M. Tignor, S. K. Allen, J. Boschung, A. Nauels, Y. Xia, V. Bex, & P. M. Midgley (Eds.), *Climate change 2013: The physical science basis. Contribution of working group I to the fifth assessment report of the Intergovernmental Panel on Climate Change* (pp. 659–740). Cambridge University Press. www.climatechange2013.org

Neubauer, D. (2016). Characterization of organic matter stored in Yedoma and thermokarst permafrost. Unpublished MSc Thesis. Freie Universität Berlin.

Nitze, I., Grosse, G., Jones, B. M., Arp, C. D., Ulrich, M., Fedorov, A., & Veremeeva, A. (2017). Landsat-based trend analysis of lake dynamics across northern permafrost regions. *Remote Sensing*, 9(7), 1–28. https://doi.org/10.3390/rs9070640

Pancost, R. D., McClymont, E. L., Bingham, E. M., Roberts, Z., Charman, D. J., Hornibrook, E. R. C., Blundell, A., Chambers, F. M., Lim, K. L. H., & Evershed, R. P. (2011). Archaeol as a methanogen biomarker in ombrotrophic bogs. *Organic Geochemistry*, 42(10), 1279–1287. https://doi.org/10.1016/j.orggeochem.2011.07.003

Poynter, J., & Eglinton, G. (1990). 14. Molecular composition of three sediments from hole 717c: The Bengal fan. *Proceedings of the Ocean Drilling Program: Scientific Results*, 116, 155–161.

Radke, M., Willsch, H., & Welte, D. H. (1980). Preparative hydrocarbon group type determination by automated medium pressure liquid chromatography. *Analytical Chemistry*, 52(3), 406–411. https://doi.org/10.1021/ac50053a009

Richardson, D. C., Newbold, J. D., Aufdenkampe, A. K., Taylor, P. G., & Kaplan, L. A. (2013). Measuring heterotrophic respiration rates of suspended particulate organic carbon from stream ecosystems. *Limnology and Oceanography: Methods*, 11(5), 247–261. https://doi.org/10.4319/lom.2013.11.247

Romankevich, E. A., Vetrov, A. A., Belyaev, N. A., Sergienko, V. I., Semiletov, I. P., Sukhoverkhov, S. V., Bratskaya, S. Y., Prokuda, N. A., & Ulyantsev, A. S. (2017). Alkanes in Quaternary deposits of the Laptev Sea. *Doklady Earth Sciences*, 472(1), 36–39. https://doi.org/10.1134/S1028334X17010093

Sánchez-García, L., Vonk, J. E., Charkin, A. N., Kosmach, D., Dudarev, O. V., Semiletov, I. P., & Gustafsson, Ö. (2014). Characterisation of three regimes of collapsing arctic ice complex deposits on the SE Laptev sea coast using biomarkers and dual carbon isotopes. *Permafrost and Periglacial Processes*, 25(3), 172–183. https://doi.org/10.1002/ppp.1815

Schädel, C., Bader, M.-F., Schuur, E. A. G., Biasi, C., Bracho, R., Čapek, P., De Baets, S., Diáková, K., Ernakovich, J., Estop-Aragones, C., Graham, D. E., Hartley, I. P., Iversen, C. M., Kane, E., Knoblauch, C., Lupascu, M., Martikainen, P. J., Natali, S. M., Norby, R. J., … Wickland, K. P. (2016). Potential carbon emissions dominated by carbon dioxide from thawed permafrost soils. *Nature Climate Change*, 6, 950–954. https://doi.org/10.1038/nclimate3054

Schädel, C., Schuur, E. A. G., Bracho, R., Elberling, B., Knoblauch, C., Lee, H., Luo, Y., Shaver, G. R., & Turetsky, M. R. (2014). Circumpolar assessment of permafrost C quality and its vulnerability over time using long-term incubation data. *Global Change Biology*, 20(2), 641–652. https://doi.org/10.1111/gcb.12417

Schirrmeister, L., Dietze, E., Matthes, H., Grosse, G., Strauss, J., Laboor, S., Ulrich, M., Kienast, F., & Wetterich, S. (2020). The genesis of Yedoma Ice Complex permafrost – Grain-size endmember modeling analysis from Siberia and Alaska. *E&G Quaternary Science Journal*, 69(1), 33–53. https://doi.org/10.5194/egqsj-69-33-2020

Schirrmeister, L., Froese, D., Tumskoy, V., Grosse, G., & Wetterich, S. (2013). *Yedoma: Late Pleistocene ice-rich syngenetic permafrost of Beringia*. In S. A. Elias, C. J. Mock, & J. Murton (Eds.). Elsevier. https://doi.org/10.1016/B978-0-444-53643-3.00106-0

Schirrmeister, L., Schwamborn, G., Overduin, P. P., Strauss, J., Fuchs, M. C., Grigoriev, M., Yakshina, I., Rethemeyer, J., Dietze, E., & Wetterich, S. (2017). Yedoma Ice Complex of the Buor Khaya

Peninsula (southern Laptev Sea). *Biogeosciences*, 14(5), 1261–1283. https://doi.org/10.5194/bg-14-1261-2017

Schuur, E. A. G., Bockheim, J., Canadell, J. G., Euskirchen, E., Field, C. B., Goryachkin, S. V., Hagemann, S., Kuhry, P., Lafleur, P. M., Lee, H., Mazhitova, G., Nelson, F. E., Rinke, A., Romanovsky, V. E., Shiklomanov, N., Tarnocai, C., Venevsky, S., Vogel, J. G., & Zimov, S. A. (2008). Vulnerability of permafrost carbon to climate change: Implications for the global carbon cycle. *BioScience*, 58(8), 701–714. https://doi.org/10.1641/B580807

Schuur, E. A. G., McGuire, A. D., Schädel, C., Grosse, G., Harden, J. W., Hayes, D. J., Hugelius, G., Koven, C. D., Kuhry, P., Lawrence, D. M., Natali, S. M., Olefeldt, D., Romanovsky, V. E., Schaefer, K., Turetsky, M. R., Treat, C. C., & Vonk, J. E. (2015). Climate change and the permafrost carbon feedback. *Nature*, 520, 171–179. https://doi.org/10.1038/nature14338

Schuur, E. A. G., Vogel, J. G., Crummer, K. G., Lee, H., Sickman, J. O., & Osterkamp, T. (2009). The effect of permafrost thaw on old carbon release and net carbon exchange from tundra. *Nature*, 459(7246), 556–559. https://doi.org/10.1038/nature08031

Soloviev, P. A. (1959). Cryolithic Zone of the Northern Part of Lena-Amga Interfluve. *Izdatel'stvo Akademii SSSR, Moscow*, p. 142 (in Russian).

Soloviev, P. A. (1973). Thermokarst phenomena and land-forms due to frost heaving in Central Yakutia. *Biuletyn Peryglacialny*, 23, 135–155.

Spencer, R. G. M., Mann, P. J., Dittmar, T., Eglinton, T. I., McIntyre, C., Holmes, R. M., Zimov, N., & Stubbins, A. (2015). Detecting the signature of permafrost thaw in Arctic rivers. *Geophysical Research Letters*, 42(8), 2830–2835. https://doi.org/10.1002/2015GL063498

Stapel, J. G., Schirrmeister, L., Overduin, P. P., Wetterich, S., Strauss, J., Horsfield, B., & Mangelsdorf, K. (2016). Microbial lipid signatures and substrate potential of organic matter in permafrost deposits: Implications for future greenhouse gas production. *Journal of Geophysical Research: Biogeosciences*, 121(10), 2652–2666. https://doi.org/10.1002/2016JG003483

Stapel, J. G., Schwamborn, G., Schirrmeister, L., Horsfield, B., & Mangelsdorf, K. (2018). Substrate potential of last interglacial to Holocene permafrost organic matter for future microbial greenhouse gas production. *Biogeosciences*, 15(7), 1969–1985. https://doi.org/10.5194/bg-15-1969-2018

Strauss, J., Laboor, S., Schirrmeister, L., Grosse, G., Fortier, D., Hugelius, G., Knoblauch, C., Romanovsky, V. E., Schädel, C., Schneider von Deimling, T., Schuur, E. A. G., Shmelev, D., Ulrich, M., & Veremeeva, A. (2020). Yedoma and Thermokarst site characteristics from sample analysis, 1998–2016, Alaska (US), Northern Siberia (RU). *Alfred Wegener Institute - Research Unit Potsdam, PANGAEA*. https://doi.org/10.1594/PANGAEA.919064

Strauss, J., Schirrmeister, L., Grosse, G., Fortier, D., Hugelius, G., Knoblauch, C., Romanovsky, V., Schädel, C., von Deimling, T. S., Schuur, E. A. G., Shmelev, D., Ulrich, M., & Veremeeva, A. (2017). Deep Yedoma permafrost: A synthesis of depositional characteristics and carbon vulnerability. *Earth-Science Reviews*, 172, 75–86. https://doi.org/10.1016/j.earscirev.2017.07.007

Strauss, J., Schirrmeister, L., Mangelsdorf, K., Eichhorn, L., Wetterich, S., & Herzschuh, U. (2015). Organic-matter quality of deep permafrost carbon – A study from Arctic Siberia. *Biogeosciences*, 12, 2227–2245. https://doi.org/10.5194/bg-12-2227-2015

Strauss, J., Schirrmeister, L., Wetterich, S., Borchers, A., & Davydov, S. P. (2012). Grain-size properties and organic-carbon stock of Yedoma Ice Complex permafrost from the Kolyma lowland, northeastern Siberia. *Global Biogeochemical Cycles*, 26(3), https://doi.org/10.1029/2011GB004104

Tanski, G., Wagner, D., Knoblauch, C., Fritz, M., Sachs, T., & Lantuit, H. (2019). Rapid CO_2 release from eroding permafrost in seawater. *Geophysical Research Letters*, 46(20), 11244–11252. https://doi.org/10.1029/2019GL084303

Treat, C. C., Natali, S. M., Ernakovich, J., Iversen, C. M., Lupascu, M., McGuire, A. D., Norby, R. J., Roy Chowdhury, T., Richter, A., Šantrůčková, H., Schädel, C., Schuur, E. A. G., Sloan, V. L., Turetsky, M. R., & Waldrop, M. P. (2015). A pan-Arctic synthesis of CH_4 and CO_2 production from anoxic soil incubations. *Global Change Biology*, *21*(7), 2787–2803. https://doi.org/10.1111/gcb.12875

Treat, C. C., Wollheim, W. M., Varner, R. K., Grandy, A. S., Talbot, J., & Frolking, S. (2014). Temperature and peat type control CO_2 and CH_4 production in Alaskan permafrost peats. *Global Change Biology*, *20*(8), 2674–2686. https://doi.org/10.1111/gcb.12572

Turetsky, M. R., Abbott, B. W., Jones, M. C., Anthony, K. W., Olefeldt, D., Schuur, E. A. G., Grosse, G., Kuhry, P., Hugelius, G., Koven, C., Lawrence, D. M., Gibson, C., Sannel, A. B. K., & McGuire, A. D. (2020). Carbon release through abrupt permafrost thaw. *Nature Geoscience*, *13*(2), 138–143. https://doi.org/10.1038/s41561-019-0526-0

Ulrich, M., Matthes, H., Schirrmeister, L., Schütze, J., Park, H., Iijima, Y., & Fedorov, A. N. (2017). Differences in behavior and distribution of permafrost-related lakes in Central Yakutia and their response to climatic drivers. *Water Resources Research*, *53*(2), 1167–1188. https://doi.org/10.1002/2016WR019267

Ulrich, M., Matthes, H., Schmidt, J., Fedorov, A. N., Schirrmeister, L., Siegert, C., Schneider, B., Strauss, J., & Zielhofer, C. (2019). Holocene thermokarst dynamics in Central Yakutia – A multi-core and robust grain-size endmember modeling approach. *Quaternary Science Reviews*, *218*, 10–33. https://doi.org/10.1016/j.quascirev.2019.06.010

Ulyantsev, A. S., Romankevich, E. A., Bratskaya, S. Y., Prokuda, N. A., Sukhoverkhov, S. V., Semiletov, I. P., & Sergienko, V. I. (2017). Characteristic of quaternary sedimentation on a shelf of the Laptev Sea according to the molecular composition of *n*-alkanes. *Doklady Earth Sciences*, *473*(2), 449–453. https://doi.org/10.1134/S1028334X17040158

Venables, W. N., & Ripley, B. D. (2002). *Modern applied statistics with S (fourth)*. Springer. http://www.stats.ox.ac.uk/pub/MASS4/

Vonk, J. E., Mann, P. J., Davydov, S., Davydova, A., Spencer, R. G. M., Schade, J., Sobczak, W. V., Zimov, N., Zimov, S., Bulygina, E., Eglinton, T. I., & Holmes, R. M. (2013). High biolability of ancient permafrost carbon upon thaw. *Geophysical Research Letters*, *40*(11), 2689–2693. https://doi.org/10.1002/grl.50348

Waldrop, M. P., Wickland, K. P., White, R. III, Berhe, A. A., Harden, J. W., & Romanovsky, V. E. (2010). Molecular investigations into a globally important carbon pool: Permafrost-protected carbon in Alaskan soils. *Global Change Biology*, *16*(9), 2543–2554. https://doi.org/10.1111/j.1365-2486.2009.02141.x

Walter Anthony, K., Daanen, R., Anthony, P., Schneider von Deimling, T., Ping, C.-L., Chanton, J. P., & Grosse, G. (2016). Methane emissions proportional to permafrost carbon thawed in Arctic lakes since the 1950s. *Nature Geoscience*, *9*(9), 679–682. https://doi.org/10.1038/ngeo2795

Walz, J., Knoblauch, C., Tigges, R., Opel, T., Schirrmeister, L., & Pfeiffer, E.-M. (2018). Greenhouse gas production in degrading ice-rich permafrost deposits in northeastern Siberia. *Biogeosciences*, *15*(17), 5423–5436. https://doi.org/10.5194/bg-15-5423-2018

Weijers, J. W. H., Schouten, S., Spaargaren, O. C., Damsté, J. S., & Sinninghe Damsté, J. S. (2006). Occurrence and distribution of tetraether membrane lipids in soils: Implications for the use of the TEX86 proxy and the BIT index. *Organic Geochemistry*, *37*(12), 1680–1693. https://doi.org/10.1016/j.orggeochem.2006.07.018

Wild, B., Schnecker, J., Alves, R. J. E., Barsukov, P., Bárta, J., Čapek, P., Gentsch, N., Gittel, A., Guggenberger, G., Lashchinskiy, N., Mikutta, R., Rusalimova, O., Šantrůčková, H., Shibistova, O., Urich, T., Watzka, M., Zrazhevskaya, G., & Richter, A. (2014). Input of easily available organic C and N stimulates microbial decomposition of soil organic matter in arctic permafrost soil. *Soil Biology and Biochemistry*, *75*, 143–151. https://doi.org/10.1016/j.soilbio.2014.04.014

Windirsch, T., Grosse, G., Ulrich, M., Schirrmeister, L., Fedorov, A. N., Konstantinov, P. Y., Fuchs, M., Jongejans, L. L., Wolter, J., Opel, T., & Strauss, J. (2020). Organic carbon characteristics in ice-rich permafrost in alas and Yedoma deposits, central Yakutia. *Siberia. Biogeosciences*, *17*(14), 3797–3814. https://doi.org/10.5194/bg-17-3797-2020

Winkel, M., Sepulveda-Jauregui, A., Martinez-Cruz, K., Heslop, J. K., Rijkers, R., Horn, F., Liebner, S., & Walter Anthony, K. M. (2019). First evidence for cold-adapted anaerobic oxidation of methane in deep sediments of thermokarst lakes. *Environmental Research Communications*, *1*(2). https://doi.org/10.1088/2515-7620/ab1042

Zech, M., Buggle, B., Leiber, K., Marković, S., Glaser, B., Hambach, U., Huwe, B., Stevens, T., Sümegi, P., Wiesenberg, G., & Zöller, L. (2009). Reconstructing Quaternary vegetation history in the Carpathian Basin, SE-Europe, using n-alkane biomarkers as molecular fossils: Problems and possible solutions, potential and limitations. *E&G Quaternary Science Journal*, *58*(2), 148–155. https://doi.org/10.3285/eg.58.2.03

Zimov, S. A., Davydov, S. P., Zimova, G. M., Davydova, A. I., Schuur, E. A. G., Dutta, K., & Chapin, F. S. (2006). Permafrost carbon: Stock and decomposability of a globally significant carbon pool. *Geophysical Research Letters*, *33*(20). https://doi.org/10.1029/2006GL027484

Zona, D., Lipson, D. A., Paw, U. K. T., Oberbauer, S. F., Olivas, P., Gioli, B., & Oechel, W. C. (2012). Increased CO_2 loss from vegetated drained lake tundra ecosystems due to flooding: Increased tundra CO_2 loss due to flooding. *Global Biogeochemical Cycles*, *26*(2). https://doi.org/10.1029/2011GB004037

SUPPORTING INFORMATION

Additional supporting information may be found online in the Supporting Information section.